PCCP

Accepted Manuscript

ROYAL SOCIETY OF CHEMISTRY

www.rsc.org/pccp

Physical Chemistry Chemical Physics
CREATED USING THE RSC LaTeX PCCP ARTICLE TEMPLATE – SEE www.rsc.org/electronicfiles FOR DETAILS
ARTICLE TYPE www. rsc.org/xxxxxx | XXXXXXXX

The interplay between interface structure, energy level alignment and chemical bonding strength at organic-metal interfaces

M. Willenbockel,[a, b] D. Lüftner,[c] B. Stadtmüller,[a, b‡] G. Koller,[c] C. Kumpf,[a, b] S. Soubatch,[a, b] P. Puschnig,[c] M. G. Ramsey,[c] and F. S. Tautz*[a, b]

Received Xth XXXXXXXXXX 20XX, Accepted Xth XXXXXXXXX 20XX
First published on the web Xth XXXXXXXXXX 200X
DOI: 10.1039/b000000x

What do energy level alignments at metal-organic interfaces reveal about the metal-molecule bonding strength? Is it permissible to take vertical adsorption heights as indicators of bonding strengths? In this paper we analyse 3,4,9,10-perylene-tetracarboxylic acid dianhydride (PTCDA) on the three canonical low index Ag surfaces to provide exemplary answers to these questions. Specifically, we employ angular resolved photoemission spectroscopy for a systematic study of the energy level alignments of the two uppermost frontier states in ordered monolayer phases PTCDA. Data are analysed using the orbital tomography approach. This allows the unambiguous identification of the orbital character of these states, and also the discrimination between inequivalent species. Combining this experimental information with DFT calculations and the generic Newns-Anderson chemisorption model, we analyse the alignments of highest occupied and lowest unoccupied molecular orbitals (HOMO and LUMO) with respect to the vacuum levels of bare and molecule-covered surfaces. This reveals clear differences between the two frontier states. In particular, on all surfaces the LUMO is subject to considerable bond stabilization through the interaction between the molecular π-electron system and the metal, as a consequence of which it also becomes occupied. Moreover, we observe a larger bond stabilization for the more open surfaces. Most importantly, our analysis shows that both the orbital binding energies of the LUMO and the overall adsorption heights of the molecule are linked to the strength of the chemical interaction between the molecular π-electron system and the metal, in the sense that stronger bonding leads to shorter adsorption heights and larger orbital binding energies.

1 Introduction

The alignment of molecular energy levels at metal-organic interfaces is important for the engineering of organic electronic devices and has been studied in great detail for many years. A large body of experimental data has been assembled, and powerful models have been developed that describe the phenomenology well [1–17].

It is clear that ultimately the energy level alignments will be determined by the atomistic structure of the interface. Evidently, this link will always be taken into account automatically when the electronic properties in general and energy level alignments in particular are calculated with atomistic first- principles methods, such as density functional theory, albeit within the error of the chosen functional. However, in many experiments on energy level alignments, the interface structure is not so well controlled, sometimes not even known, and it is therefore often difficult to establish the link between electronic and geometric structures on the basis of the available experimental data.

Of course, there is also a large body of experimental work focussing on interface structures [18–20] , but in our view the systematic connection between electronic and geometric structure of these interfaces has not been investigated sufficiently so far, since the majority of previous works, including our own, have – with a few notable exceptions (e.g. [21,22]) – focussed on *either* electronic *or* atomic structure, at the expense of the respective other. Here we attempt a discussion of both aspects on the same footing.

To approach this goal, we study in this paper the electronic structure of the 3,4,9,10-perylene-tetracarboxylic acid dianhydride (PTCDA) molecule on the three canonical low index Ag surfaces. This material system PTCDA/Ag(*hkl*) is ideally suited to attempt a comprehensive and unified view of geometric and electronic interface structures, because a complete set of lateral and vertical structural data is available for these interfaces and has been published, see e.g. Bauer et al. [23]. Moreover, there are large variations in the surface reactivity of these three surfaces, allowing us to study how this parameter influences geometric and electronic interface structures.

[a] *Peter Grünberg Institut (PGI-3), Forschungszentrum Jülich, 52425 Jülich, Germany.*
[b] *Jülich Aachen Research Alliance (JARA)–Fundamentals of Future Information Technology, 52425 Jülich, Germany.*
[c] *Institut für Physik, Karl-Franzens-Universität Graz, 8010 Graz, Austria.*
* *E-mail: s.tautz@fz-juelich.de*
‡ *Present address: Department of Physics and Research Center OPTIMAS, University of Kaiserslautern, Erwin-Schroedinger-Strasse 46, 67663Kaiserslautern, Germany.*

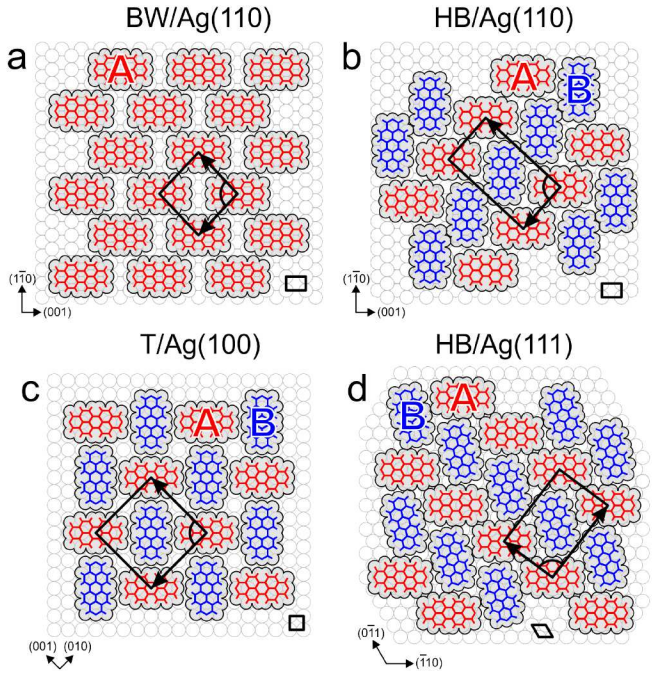

Fig. 1 Structure models of monolayer PTCDA phases. (a) Brickwall phase of PTCDA/Ag(110)[24–26]. (b) Herringbone phase of PTCDA/Ag(110)[27–30]. (c) T-phase of PTCDA/Ag(100)[31]. (d) Herringbone phase of PTCDA/Ag(111)[32]. For HB/Ag(111), only one of six symmetry-equivalent domains is shown. A- and B-molecules are marked in red and blue, respectively.

Below, we present electronic structure data in the form of energy level alignments of the two uppermost frontier orbitals of PTCDA in four different bonding configurations on three Ag surfaces, also resolving different surface species within the unit cell where applicable with the help of the orbital tomography technique. On this basis we attempt a comprehensive discussion of interfacial energy level alignments in the light of atomistic interface structures. Thereby, our goal is relating the observed energy level alignments to measured interface structures and ultimately to the molecule-substrate bonding strengths found at the respective interfaces.

Our aim is developing a conceptual understanding of interface structure, energy level alignment and chemical bonding and their interplay, using PTCDA/Ag(*hkl*) monolayers as an illustrative examples. Therefore, the discussion includes both empirical findings, first-principles calculations and a generic model of chemisorption in order to provide the sought-after conceptual insight. We believe that, although results and discussion presented here are specific to PTCDA/Ag(*hkl*), they nevertheless reveal trends that can be generalized to other molecule/metal combinations, in particular those which, like PTCDA on silver, can be classified as weakly chemisorbing.

2 Experimental and theoretical methodology

2.1 Experiment

Because of the limited bias range of scanning tunneling spectroscopy (STS) around the Fermi level and because of the residual tip influence on the STS spectra, we have chosen photoelectron spectroscopy (PES) as our experimental method. However, there are two shortcomings of standard PES: Firstly, in a photoemission experiment with fixed detection angle at which the photoelectrons are collected, transition probabilities may emphasize or suppress certain states, depending on experimental conditions and molecular arrangement. Therefore, individual experimental energy distribution curves (EDC) cannot be interpreted as a density of states (DOS). Secondly, because it is an ensemble averaging method, it is not straightforward to distinguish (purely experimentally, without component fitting) between different surface species of the same adsorbate. However, we know that some of the monolayer structures which PTCDA forms on low index silver surfaces contain two non-equivalent molecules in the unit cell, which, moreover, have been proven to exhibit different HOMO (highest occupied molecular orbital) and LUMO (lowest occupied molecular orbital) binding energies[27,33,34]. The question hence arises how these different binding energies can be measured in PES, without any input from theory.

It has been shown recently that the above-mentioned shortcomings of PES can be partially overcome by performing angle resolved PES[28,35–38]. Collecting photoelectrons in the complete half-space above the sample surface, 'accidental' suppressions or enhancements of the photoelectron intensitiy can be excluded. Moreover, because the angular (i.e. in-plane momentum k_x and k_y) distribution of photoelectrons is related to the Fourier transform of the emitting orbital, molecules with different orientations on the sample surface can be distinguished. If the different surface species in a given unit cell also differ by their in-plane orientations (and this is the case for the PTCDA phases in question), the orientation of the Fourier transform, can be used to distinguish the different surface species from each other. In this way, the energy level alignments of individual surface species can be determined[33,36,38].

Our angle resolved photoemission spectroscopy (ARPES) experiments were carried out at the Helmholtz-Zentrum Berlin (BESSY II storage ring, Beamline U125/2-SGM). All experiments were conducted at room temperature under UHV conditions with a base pressure $< 2 \times 10^{-9}$ mbar. The Ag(100), Ag(110) and Ag(111) samples were cleaned by several cycles of Ar-ion sputtering and annealing up to 800 K. PTCDA molecules were evaporated from a Knudsen cell onto Ag(100), Ag(110) and Ag(111) samples at room temperature. Before loading the molecular material into the Knudsen cell, it was

Table 1 Structure parameters of the ordered monolayer phases of PTCDA on low index surface of silver that are studied in this work. Cf. ref.[27,31,32,34].

PTCDA monolayer phase	unit cell	number of molecules in unit cell	orientation of molecules
BW/Ag(110)	a_1=11.9 Å, a_2=11.9 Å 86.7° commensurate	1	along[001]
HB/Ag(110)	a_1=21.23 Å, a_2=11.65 Å 91.08° incommensurate	2	A: along[001] B: along [1$\bar{1}$0]
T/Ag(100)	a_1=16.34 Å, a_2=16.34 Å 90° commensurate	2	A: along[001] B: along [1$\bar{1}$0]
HB/Ag(111)	a_1=19.0 Å, a_2=12.6 Å 89° commensurate	2	A: along[0$\bar{1}$1] B: misaligned by 17°

purified by repeated re-sublimation. The evaporation flux was calibrated with a quartz microbalance before and controlled by a quadruple spectrometer during deposition, allowing high reproducibility of total adsorption doses of PTCDA.

After deposition, surface order was checked with low energy electron diffraction (LEED). LEED experiments were done with a multi-channel plate LEED, using typical beam currents of 1 nA to prevent the molecular film from being damaged by the electron beam.

In our ARPES experiments the samples were illuminated with 35 eV photons under an incident angle of 40° with respect to the surface normal using in-plane polarized light. The photoelectrons were recorded with a toroidal electron analyzer. This analyzer allows the simultaneous detection of photoelectrons emitted with polar angles between ±80°, with kinetic energy differences up to 2 eV and without any change of the incident light polarisation. Its energy resolution is approximately 150 to 200 meV in the present experimental conditions. To collect photoelectrons in the full hemisphere above the sample surface, the sample was rotated around its surface normal in steps of 1°. The range of azimuthal rotation was chosen for each particular experiment, taking into account the symmetry of used Ag surface, and in order to avoid artifacts caused by absorption of the reflected ultra violet beam inside the analyzer. Additionally, the photon energy was varied in different experiments in the range of (30-35) eV to improve the beam focusing and suppress reflection-caused artifacts. For more details on the toroidal analyzer see [39].

Converting the polar and azimuthal photoelectron take-off angles into parallel momentum (k_x, k_y), we obtain a three-dimensional data cube of the PE signal $I(E_B, k_x, k_y)$. This data cube can be deconvoluted using the expected momentum maps $\phi(k_x, k_y)$ of gas phase molecules [38]. The $\phi(k_x, k_y)$ can be determined as squares of the Fourier transform of real space orbitals as predicted by density functional calculations of the gas phase molecule [35,36]. In this way, experimental orbital projected partial densities of states can be derived [38].

2.2 Theory

All theoretical results presented in this work have been obtained within the framework of density functional theory (DFT) using the generalized gradient approximation (GGA) [40] to account for exchange-correlation effects.

In order to calculate constant binding energy (CBE) momentum maps of an isolated PTCDA molecule (insets in Fig. 2), which are necessary for the k-space deconvolution of experimental ARPES $I(E_B, k_x, k_y)$ data cubes to obtain experimental partial densities of states (PDOS) of HOMO and LUMO on the different Ag surfaces, we utilized the plane wave code ABINIT [41]. The all-electron potentials were replaced by extended norm-conserving, highly transferable Troullier-Martins pseudo potentials [42] using a plane wave cut-off of 50 Ryd. We employed a super cell approach with a box size of $50 \times 50 \times 22$ Bohr^3 and Γ point sampling of the Brillouin zone. The geometry of the free molecule was optimized by using GGA [40] for exchange-correlation effects.

For the computation of theoretical PDOS (Fig. 7), charge density profiles (Fig. 4.3), work functions (Table 3, Fig. 8) and adsorption energies (Fig. 12) of PTCDA on Ag(110), Ag(100) and Ag(111) we employed a repeated slab approach using the VASP code [43,44]. The substrate was modeled by 6 metallic layers with an additional vacuum layer of ≈ 15 Å. In addition, for each surface we performed calculations of a freestanding molecular layer and the bare Ag substrate, using the same geometry, energy cut-off and k-point grid as for the PTCDA/Ag

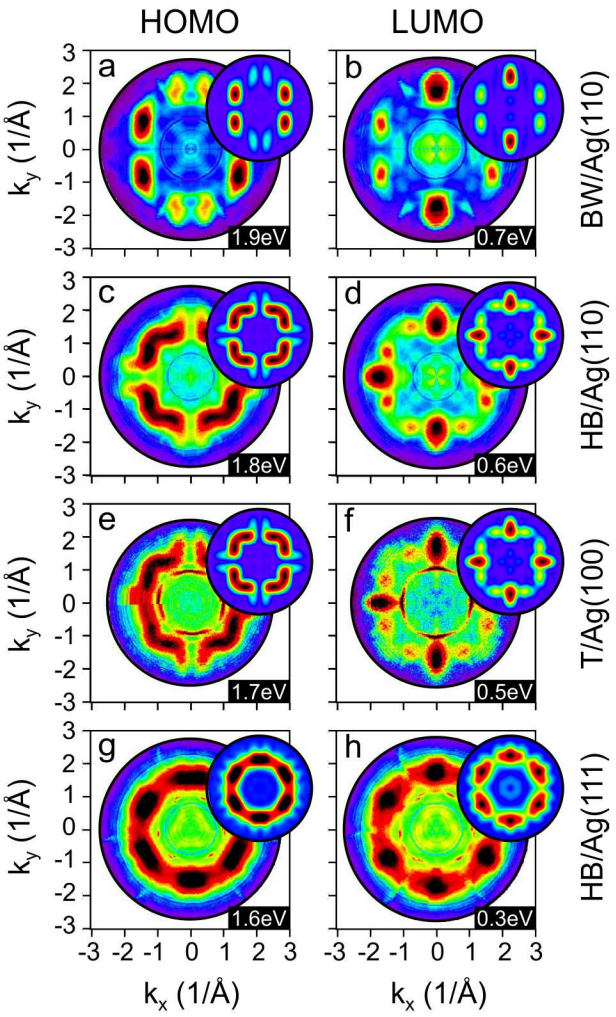

Fig. 2 Experimental CBE momentum maps obtained at the indicated binding energies E_B corresponding to maximum intensity of the HOMO (left panel) and LUMO (right panel) for four PTCDA monolayer phases. Insets show calculated CBE maps summed for A and B molecules in the corresponding structures. Note that in some cases differences in E_B between A and B molecules are already obvious (e.g. panel d, see main text).

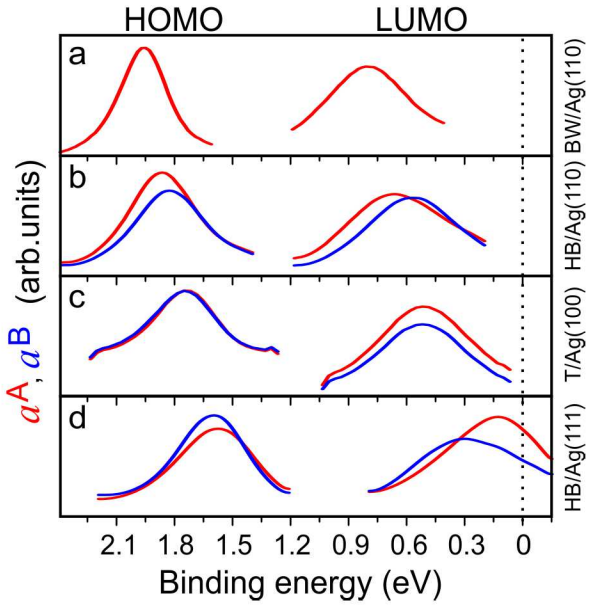

Fig. 3 Experimental partial density of states (PDOS) of HOMO and LUMO in (a) BW/Ag(110)[38], (b) HB/Ag(110)[27], (c) T/Ag(100), and (d) HB/Ag(111)[33] monolayer phases of PTCDA, based on $I(E_B, k_x, k_y)$ data cube deconvolution in k-space (see text for more details). In (b-d), the red (blue) curves correspond to molecules A (B). Binding energy zero corresponds to the Fermi level.

systems. The projector augmented waves (PAW)[45] approach was used, allowing for a relatively low kinetic energy cut-off of about 350 eV. We employed a Monkhorst-Pack $6 \times 6 \times 1$ grid of k-points for PTCDA/Ag(110) and a $3 \times 3 \times 1$ grid for PTCDA/Ag(100) and PTCDA/Ag(111)[46], and a first-order Methfessel-Paxton smearing of 0.2 eV[47]. To avoid spurious electrical fields, a dipole layer was inserted in the vacuum region[48]. For the Ag lattice constant we used a GGA optimized value of 4.16 Å. During the geometry optimization of the internal atomic positions we fixed the height of the carbon atoms of the molecule at the experimentally obtained value above the surface and allowed for relaxations of the other atoms of the molecule as well as the two topmost layers of the metal substrate. Van der Waals interactions which are ill-described in standard GGA functionals[49–52] were accounted for by the empirical correction scheme according to Grimme[53].

In order to determine the work functions Φ_0^{hkl} and Φ^{hkl} of bare and molecule-covered surfaces, respectively, we have computed laterally averaged electrostatic (no exchange-correlation contributions) potentials as a function of the z-coordinate normal to the surface. The contribution to the work function change that arises from the bond dipole between PTCDA and the substrate, $\Delta\Phi_{bond}$, was calculated from the charge density difference between the interacting system ($\rho_{tot}(r)$) and the corresponding separated systems ($\rho_{mol}(r)$,

$\rho_{substrate}(r)$) via

$$\Delta\rho(r) = \rho_{tot}(r) - (\rho_{mol}(r) + \rho_{substrate}(r)), \quad (1)$$

where for the calculation of $\rho_{mol}(r)$ and $\rho_{substrate}(r)$ the atoms were frozen in the geometry of the $\rho_{tot}(r)$ calculation. Solving the one-dimensional Poisson equation for this charge density difference we obtained changes in the potential induced by the bond dipole formation upon adsorption (red-blue dashed line in Fig. 8a). The second contribution to the work function change $\Delta\Phi_{bend}$, due to the bending of the molecule upon adsorption, was calculated as the difference of the laterally averaged electrostatic potential above and below the freestanding PTCDA monolayer (dashed cyan line of Fig. 8b)[54].

3 Results

3.1 Surface structures

In this paper, four different monolayer films have been investigated. These are the herringbone (HB) phase on Ag(111) [32] , the T-phase on Ag(100)[31], the brickwall (BW) phase on Ag(110)[24–26] and the HB phase on Ag(110)[27–30]. Structure parameters of these phases are summarized in Table 1 and the corresponding unit cells are plotted in Fig. 1. While the BW/Ag(110) monolayer consists of parallel molecules and has one molecule per unit cell, the HB/Ag(110), HB/Ag(111) and T/Ag(100) monolayers have two differently oriented PTCDA molecules in their unit cells.

We denote the two differently oriented molecules in these three monolayer films as A and B according to following notation (see Fig. 1): (1) for HB/Ag(110), the A-molecule is the one oriented along [001], i.e. the one with the same orientation as in the BW/Ag(110), while the B-molecule is oriented along $[1\bar{1}0]$, i.e. perpendicular to A; (2) for T/Ag(100), the choice of A and B is arbitrary, because both molecules in the unit cell are identical by symmetry; (3) for HB/Ag(111), the A-molecule (also referred to as the aligned molecule[34]) is almost perfectly aligned along $[10\bar{1}]$; the B-molecule (also referred to as misaligned[34]) is rotated 17° away from $[10\bar{1}]$, yielding a rotation of 77° relative to the A-molecule[55]. Energy levels of the HB/Ag(111)[33,34,55], the HB/Ag(110)[27] and the BW/Ag(110)[38] have been reported before. Here, we present new data for the T/Ag(100) and discuss systematic trends between all four surfaces.

3.2 Angle resolved photoemission spectroscopy

Fig. 2 shows cross sections through measured data cubes $I(E_B,k_x,k_y)$, i.e. constant binding energy (CBE) momentum maps, at binding energies E_B near to those of the HOMO and the LUMO for the respective films. Since molecules with different in-plane orientations are present in the films (except for BW/Ag(110)), the experimental CBE momentum maps have to be compared to superpositions of calculated $\phi(k_x,k_y)$ maps for the respective orientations. The corresponding superpositions are shown as insets in Fig. 2. It can be seen that the measured distributions fit well to the predicted ones. While only one molecular orientation is present in the map of BW/Ag(110)[37,38] , the maps of T/Ag(100) and HB/Ag(110)[27] can each be decomposed into two nearly perpendicular orientations. The map HB/Ag(111) has multiple orientations[33], due to the combination of two molecular types with altogether 6 domains (three rotational domains, each of which has an additional mirror domain associated with it) .

Close inspection reveals that the experimental intensities for the different molecular orientations within one film may peak at different binding energies. For example, this can be observed in Fig. 2d where at the given binding energy the side lobes on the left and the right (one orientation) are stronger than the corresponding peaks at the top or the bottom (the other orientation). Therefore, in deconvoluting the data cube for each film in k-space and energy we have to take the possibility of differential binding energy shifts between molecules of different orientations into account. This can be achieved by minimizing the quantity[33,38]

$$\iint dk_x dk_y (I(E_B,k_x,k_y) - (a^A(E_B)\phi^A(k_x,k_y) + a^B(E_B)\phi^B(k_x,k_y)))^2,$$

allowing the deconvolution of the angle-dependent PES signal $I(E_B,k_x,k_y)$ into contributions $\phi^A(k_x,k_y)$ of A-molecules and $\phi^B(k_x,k_y)$ of B-molecules, thereby experimentally determining the PDOS $a^A(E_B)$ and $a^B(E_B)$ for A- and B-molecules separately.

Such (k_x,k_y,E_B)-deconvolution has already been reported for BW/Ag(110)[38], HB/Ag(110)[27] and HB/Ag(111)[33]. Their experimental PDOS are displayed in Fig. 3a, b, and d, together with the new data for T/Ag(100) in Fig. 3c. In Table 2 all binding energies are listed. On all surfaces studied here, the LUMO is filled by charge transfer from the metal upon adsorption[56]. The binding energies in Table 2 are in good agreement with the literature where they exist (see table caption).

4 Discussion

4.1 Differential shifts of orbital binding energies

Before analysing the average orbital binding energies on the three surfaces in comparison, we briefly discuss the binding energy differences between A- and B-species on one and the same surface. Fig. 3 and Table 2 show that for HB/Ag(110) and HB/Ag(111) A- and B-molecules have slightly different binding energies. If the same analysis is carried out for

Table 2 Binding energies of electronic levels for different ordered monolayer phases of PTCDA. These should be compared to the following literature values: BW/Ag(110): HOMO 1.8 eV, LUMO 0.6 eV[59]; HB/Ag(111): HOMO 1.6 eV, LUMO 0.3 eV[59]; Bulk values: HOMO 2.52 eV, LUMO -1.26 eV[60–62].

PTCDA monolayer phase	HOMO of A (eV)	HOMO of B (eV)	LUMO of A (eV)	LUMO of B (eV)	averaged HOMO (eV)	averaged LUMO (eV)	LUMO-HOMO gap (eV)	HOMO A-B offset (eV)	LUMO A-B offset (eV)
BW/Ag(110)	1.93		0.75		1.93	0.75	1.18		
HB/Ag(110)	1.89	1.85	0.69	0.60	1.87	0.645	1.225	0.04	0.09
T/Ag(100)	1.69	1.70	0.46	0.47	1.695	0.465	1.23	-0.01	-0.01
HB/Ag(111)	1.56	1.60	0.13	0.30	1.58	0.215	1.365	-0.04	-0.17

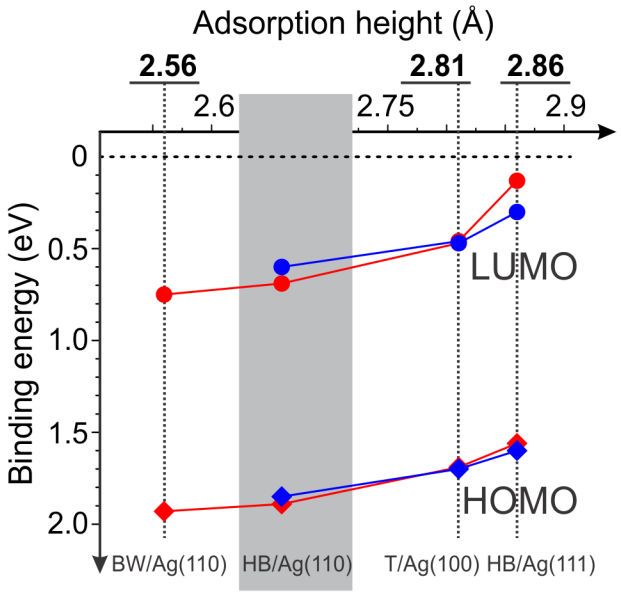

Fig. 4 Experimentally observed orbital binding energies of HOMO and LUMO as a function measured average adsorption height of the carbon skeleton of PTCDA. Binding energy zero corresponds to the Fermi level. The plot is based on adsorption height data for BW/Ag(110)[23,57], T/Ag(100)[23] and HB/Ag(111)[58]. For the incommensurate HB/Ag(110) phase, no adsorption height data is available. This is indicated by the grey shading.

T/Ag(100) (Fig. 3c), we find that $a^{\mathrm{A}}(E_{\mathrm{B}})$ and $a^{\mathrm{B}}(E_{\mathrm{B}})$ are essentially identical. Since in this structure both molecules are located on the same lattice sites and the square symmetry of the unit cell implies that both molecules also have identical neighbourhoods, it is reassuring that the deconvolution in k-space yields identical HOMO and LUMO peak positions for A- and B-molecules. This result confirms the validity of the deconvolution process.

Remarkably, for HB/Ag(110) the molecule that is aligned with a high symmetry direction of the substrate has the larger HOMO and LUMO binding energies, while for HB/Ag(111) the opposite is true. Note that the A/B splittings in HB/Ag(110) and HB/Ag(111) are small in relation to the binding energy shifts from surface to surface. It has been shown that intermolecular interactions play a dominant role for differential shifts of HOMO and LUMO within one surface structure. In particular, for HB/Ag(110) the split is mainly due to electrostatic intermolecular interactions[27], while for HB/Ag(111) a combination of intermolecular and molecule-substrate effects was proposed as the origin of the split[55].

4.2 Empirical relations, surface reactivity and work function

We start our analysis of PTCDA/Ag interfaces with stating empirical observations: The openness of the surface seems to control orbital binding energies E_{B} of HOMO and LUMO, because in the sequence (111) → (100) → (110), i.e. from the most close-packed to the most open surface, E_{B} increases. At the same time, the surface openness appears to influence the molecular adsorption heights, which decrease in the same sequence from 2.86 ± 0.01Å[58] via 2.81 ± 0.02Å to 2.56 ± 0.01Å[23,57]. As a consequence of these two tendencies, adsorption heights and orbital binding energies are also linked, in the sense that smaller adsorption heights go along with larger orbital binding energies (cf. Fig. 4). The question arises whether this link between surface openness on the one hand and adsorption height and orbital binding energies on the other is a mere coincidence, or whether there is a physical

mechanism behind it? Similarly, is it permissible to connect the adsorption height to the chemical interaction strength at the interface?

These questions bring us to the issue of surface reactivity which might be the controlling factor behind both adsorption height and energy level alignment and determine the chemical bonding strength. In non-solid state chemistry the reactivity between a pair of educts is determined by the relative energies of the frontier orbitals, which are summarised by their respective ionisation potentials (I) and electron affinities (E^{A}). These energies are based on the vacuum level as the common alignment level. For molecules adsorbing on and reacting with solid surfaces, like in the present case, this reference level becomes problematic. For different surfaces of the same solid, as considered here, the general belief is that more open surfaces are more reactive due to more bonding possibilities. For interactions with small molecules this seems reasonable, however, for larger molecules with spatially delocalized frontier orbitals it is not so obvious why an open surface should be more reactive. There is, however, a direct relationship between the openness of a surface and its work function, the latter often being considered as the solid state equivalent of the ionization potential of the gas phase. Due to the finite size of the sample crystal its reference is, however, not the vacuum level at infinity but rather the maximum of the potential created by the surface dipole due to the spill out of charge from the surface. As such, it is not an absolute but rather will vary with the approach of the molecule and the various interactions it makes with the surface. This complicates the analysis of surface reactivity and bonding strengths and how they influence observables such as adsorption height and energy level alignments.

Before analysing the role played by the work function for energy level alignment, chemical bonding strength and adsorption height in detail in sections 4.5 to 4.8, let us attempt a first analysis of what determines both the adsorption height and the energy level alignment.

4.3 What determines molecular adsorption heights?

At an intuitive level, the general tendency of a larger adsorption height for higher work function metal surfaces can be easily understood, because for a given material the work function of a metal surface is determined by the electron spill out in front of the surface. Electrons spill out of the metal surface further the more close-packed the surface is. This can be seen in Fig. 5 where laterally averaged electronic charge density profiles, as calculated in DFT are plotted as a function of z. The more extended the spill out, the larger is the work function. If we assume that the adsorption height is in zeroth order determined by the contact distance between the surface and the molecule (i.e. if the molecule *floated* above the surface in contact), we would expect larger adsorption distances for surfaces with larger work function, as is indeed observed. Moreover, a comparison of Fig. 5 with Fig. 4 shows a remarkable agreement in the sense that both the adsorption height and the spill out for Ag(110) are noticably smaller than for the other two surfaces, where the corresponding values are more similar but still show the expected tendency.

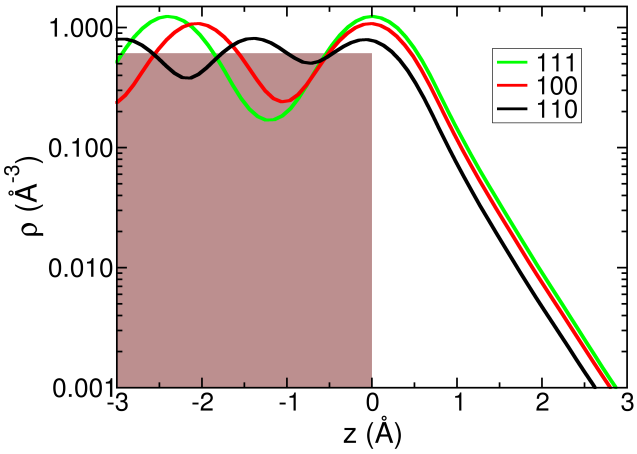

Fig. 5 Logarithmic plot of laterally averaged electronic charge densities of the Ag(111) (green), Ag(100) (red), and Ag(110) (black) surfaces (colour coding as in Fig. 6), calculated by DFT-GGA and plotted versus the z-coordinate normal to the surface. The grey box indicates the averaged positive charge background.

However, when the molecule approaches the surface the so-called pushback effect, hybridization of metal states with molecular orbitals and charge transfer will modify the spill out profile above the bare surface. This reorganization depends on the chemical character of the molecule and the balance between chemisorption and physisorption for the given interface and may well have a decisive influence on the resultant adsorption height. For this reason, the molecule is *not* just floating in contact on the unmodified spill out cloud, and hence the above mentioned relation between the work function and the adsorption height cannot be understood fully in these simple terms. Indeed, it was shown in ref.[23] that on the three different Ag surfaces spatial charge reorganization and buckling of both molecule and surface occur to very different degrees. Hence, the molecule does *react chemically* with the surface, and judging from the structural and electronic data this reaction is strongest for the Ag(110) and weakest for the Ag(111) surface (the different degree of reaction is also indicated by the different lateral structures that are formed by PTCDA on the three surfaces; it should also be noted in this context that lateral structures may also have a secondary effect on the adsorption height, too[63]).[64]

The importance of a chemical reaction is also indicated

by comparing the adsorption heights of PTCDA on the three close-packed noble metal surfaces Ag(111), Cu(111), and Au(111). The analysis in ref.[58] has shown that the adsorption distances, if corrected by the van der Waals radii of the substrates, obey a linear relationship with the work function of the bare substrate (see also Fig. 6). Assuming that the van der Waals radii, which for Ag and Au were derived from the volume of metallic liquids[65,66], while the value for Cu is based on X-ray data[65,67], take into account the expanse of the charge spill out for a given surface geometry at least to some extent, one would expect nearly constant reduced heights for the three surfaces if the molecules just floated on top of the spill out layer. But one observes substantially shorter reduced adsorption distances for Ag and Cu (in that order) than for Au. This indicates that on Ag and Cu there is a chemical reaction going on, i.e. the simple picture of the charge spill out controlling the adsorption height is incomplete. However, it is remarkable that the degree of deviation from this floating picture is again controlled by the work function. A natural explanation for this will be given in section 4.8.2.

4.4 What determines orbital binding energies?

The simplest situation is the so-called *vacuum level alignment* or Schottky-Mott regime, in which the frontier energy level alignments at an organic-metal interface can be predicted from the value of the bare metal work function Φ_0^{hkl} and the molecular electron affinity E_0^{A} and ionization potential I_0 as $E_{\mathrm{B}}^{\mathrm{LUMO}} = \Phi_0^{hkl} - E_0^{\mathrm{A}}$ and $E_{\mathrm{B}}^{\mathrm{HOMO}} = \Phi_0^{hkl} - I_0$.

Vacuum level alignment denotes the situation that arises when the vacuum level of the molecule $E_{\mathrm{vac}}^{\mathrm{mol}}$, to which I_0 and E_0^{A} are referenced, is aligned to the vacuum level E_{vac}^{hkl} in front of the surface, to which its work function Φ_0^{hkl} is referenced. In other words, as the molecule approaches the surface, its vacuum level $E_{\mathrm{vac}}^{\mathrm{mol}}$ 'rides' on the electrostatic potential outside the crystal, which for distances d of the order of the linear crystal dimensions L converges to a common level, but for intermediate distances $a \ll d \ll L$, where a is a typical interatomic distance, acquires a characteristic value E_{vac}^{hkl} for each surface orientation. The vacuum level alignment approximation is justified by the fact that if the molecule is not interacting too strongly with the metal and no molecule-induced surface dipole is set up, i.e. for $d \gg a$, the energy required to move an electron from the metal through the surface into the neutral molecule is $\Phi_0^{hkl} - E_0^{\mathrm{A}}$, while the transfer of one electron from the neutral molecule through the surface into the metal needs $I_0 - \Phi_0^{hkl}$. In the vacuum level alignment regime we would expect the binding energies of the molecular states to increase linearly with decreasing substrate work function. This trend, but not perfectly linearly, is indeed observed in Fig. 3.

However, at most organic-metal interfaces, including the ones studied here, the situation in considerably more complex. First, the pushback effect will influence the metal's charge spill out and in this way induce an interface dipole, with the result that a step occurs between the vacuum levels of the metal and the molecular layer. This modifies the overall work function of the system. Note that despite breaking the vacuum level alignment the molecular energy levels may under certain circumstances still remain pinned to the vacuum level (see below). Secondly, further changes in the work function and the level alignment will be instigated by a possible charge transfer between metal and molecular layer. In the present case of PTCDA on Ag surfaces, we know that charge transfer is taking place, albeit to different degrees for the three surface orientations, because the affinity level (LUMO) becomes occupied on adsorption.

Charge transfer at metal-organic interfaces is often discussed in terms of an induced density of interface states (IDIS) and a molecular charge neutrality level (CNL)[16], the idea being that by the interaction with the substrate (hybridization, chemical bonding) the discrete molecular levels are broadened into a continuous IDIS. The charge state of the molecule is then determined by the integration of the IDIS up to the common Fermi level of metal and organic layer. Thereby the CNL defines the position of the common Fermi level at which the interacting molecular layer would remain charge neutral. In this model, the level alignment is determined by the equilibration of the chemical potential across the organic-metal interface. Initially, the neutral molecule approaches the surface and the pushback effect leads to the formation of a specific step between the vacuum levels of substrate and molecular layer and the corresponding level alignment at the interface. If after this initial step the Fermi level of the metal and the CNL of the charge neutral molecular layer are not aligned, then charge will flow into or out of the IDIS until the chemical potentials in the metal and the molecular layer are equilibrated. This charge flow will create an additional interface dipole that tends to bring the CNL and Fermi level in the metal into line; how closely they actually are able to align depends on the size of the IDIS. If the IDIS is sufficiently large, the molecular layer can provide or accept enough charge to bring the metal Fermi level in line with itself. This is the so-called *Fermi level pinning* regime, in which the energy levels of the molecule are pinned to the Fermi level irrespective of the work function of the metal.

In reality, the behaviour of most systems will be found somewhere in between the two limiting cases of Fermi level pinning and vacuum level pinning. To quantify their behaviour, it is customary to define the so-called screening parameter $S^{\mathrm{MO}} = dE_{\mathrm{B}}^{\mathrm{MO}}/d\Phi$, where $E_{\mathrm{B}}^{\mathrm{MO}}$ is the binding energy of either HOMO or LUMO. For vacuum level pinning $S = -1$, i.e. the level in question follows the work function, although there may be a step in the vacuum level due to the pushback effect, while Fermi level pinning has $S = 0$ (We note that our

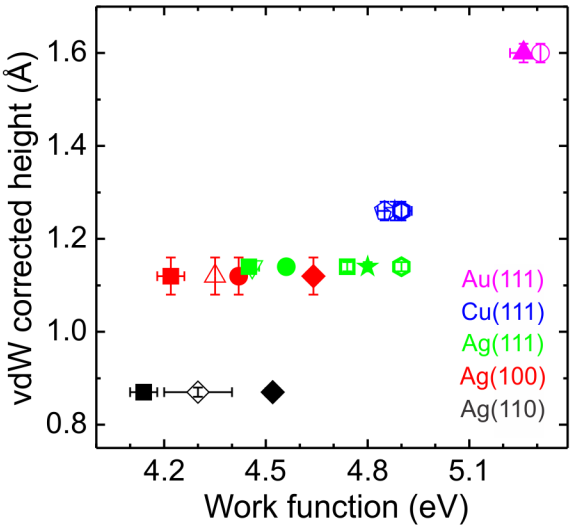

Fig. 6 Reduced adsorption heights $d_c^{\mathrm{vdW}} = d_c - r_{\mathrm{substrate}}^{\mathrm{vdW}}$, where d_c is the adsorption height of PTCDA's carbon backbone and $r_{\mathrm{substrate}}^{\mathrm{vdW}}$ is the van der Waals radius of the metal substrate, plotted versus measured work functions. The plot is an extended version of the one presented in reference [58]. Work function data are taken from: solid triangle - ref. [68], open circle - ref. [69], open pentagon - ref. [70], open star - ref. [71], open hexagon - ref. [72], open square - ref. [73], solid square - ref. [74], solid circle - ref. [75], open downward triangle - ref. [76], solid star - ref. [59], solid rhombus - ref. [77], open triangle - ref. [78], open rhombus - ref. [79]. Height data are taken from: ref. [23,57,80–82]. The following van der Waals radii were used for calculating the reduced adsorption heights: Ag - 1.72 Å, Au - 1.66 Å, Cu - 1.4 Å [65].

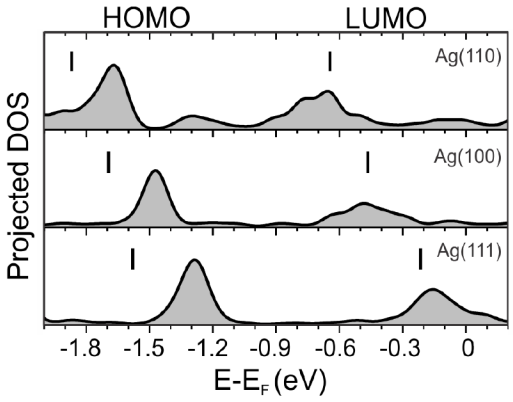

Fig. 7 Calculated partial densities of state (PDOS), projected onto the PTCDA molecule, for the three commensurate structures BW/Ag(110), T/Ag(100) and HB/Ag(111). For details of the DFT calculations, refer to section 2.2. Vertical bars indicate the experimental binding energies, averaged between A and B molecules where applicable.

convention of defining binding energies of levels below the Fermi level as positive leads to negative S-parameters). The so-called 'Schottky-Mott limit' corresponds to $S = -1$ and the absence of the pushback effect. Note that values $S < -1$ are impossible in the IDIS model, as this would mean that with respect to the metal Fermi level the orbital shifts faster than the vacuum level, but in the above model charge transfer will always screen the effect of the work function on the binding energy of the level, never amplify it.

In section 4.7 we will analyse the S-parameters for HOMO and LUMO and find that both levels behave differently. The behaviour of the LUMO actually falls outside the bounds of the IDIS model.

4.5 Work function

In the two previous sections we have seen that the work function is a central quantity both for determining the adsorption height and the energy level alignment at an organic-metal interface. For this reason, we now turn to a detailed analysis of work functions in the PTCDA/Ag system. Fig. 6 contains reported experimental work functions of the three bare Ag surfaces, together with the reduced adsorption heights of PTCDA (carbon skeleton) on these surfaces. One observes a strong experimental scatter of measured work functions, reflecting the sensitivity of this area-averaged quantity to surface preparation. Yet, the tendency that the work function of bare Ag surfaces increases in the sequence $(110) \rightarrow (100) \rightarrow (111)$ is clear. However, for a quantitative analysis of the HOMO and LUMO energy level positions the experimental work function data is not of sufficient accuracy. We therefore turn to theory. It has been shown before that theory is able to predict reasonably accurate values of the work function [22,49]. Moreover, as Fig. 7 shows, DFT predicts HOMO and LUMO level positions in good agreement with experiment, such that experimental data on level positions and theoretical data on work functions can be combined for the purpose of the present discussion. Because the HB/Ag(110) interface is incommensurate, we have no work function data from theory. This film is therefore excluded from the following discussion.

Table 3 contains calculated work functions for bare and PTCDA-covered Ag(hkl) surfaces. The work function of the bare substrates has been determined at the bottom surface of the PTCDA/Ag slab. We observe the expected tendency of increasing work function with atomic density in the sequence $(110) \rightarrow (100) \rightarrow (111)$ for the bare Ag surfaces.

On all three surfaces DFT predicts an increase of the work function as a PTCDA monolayer is adsorbed. For BW/Ag(110) this is illustrated in Fig. 8. Table 3 also shows how the work function change on adsorption $\Delta\Phi$ can be partitioned between different mechanisms. Firstly, there is the

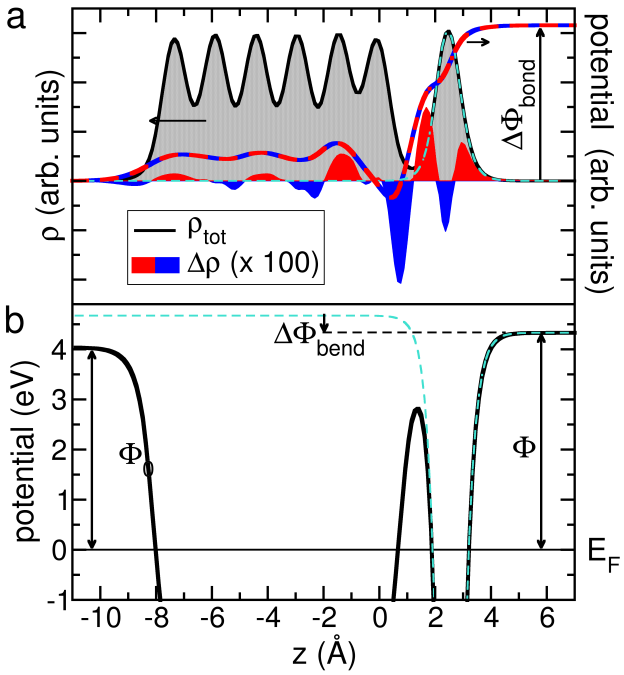

Fig. 8 (a) Black line (left axis): Charge density profile of the six layer Ag(110) slab with adsorbed PTCDA in BW structure (right). Blue and red histograms (left axis) indicate the difference in charge density between the interacting and non-interacting systems (multiplied by a factor of 100 with respect to the black curve). Red indicates electron accumulation, blue electron depletion. The red-blue dashed line (right axis) is obtained by integrating the charge difference twice; it shows the laterally averaged electrostatic potential as a function of z. Note that the red-blue dashed line does not include the bend dipole, because the non-interacting reference layer exhibits the same molecular distortion as the interactinf layer. (b) Laterally averaged electrostatic potential for BW/Ag(110) (black line) and for a free-standing BW layer of PTCDA (dashed cyan line) in the adsorption geometry, including molecular distortions, referenced to the Fermi level E_F.

Table 3 Work functions and potential steps from DFT. Φ_0: work function of Ag(*hkl*), determined at the bottom side of PTCDA/Ag slab; Φ: work function of PTCDA/Ag(*hkl*); $\Delta\Phi_{bond}$: work function change due to electron density rearrangements upon adsorption (bond dipole); $\Delta\Phi_{bend}$: potential difference below and above the PTCDA layer for the PTCDA/Ag(*hkl*) system (dipole due to molecular distortion); $\Delta\Phi_{Ag}$, potential difference below and above Ag layers for the PTCDA/Ag(*hkl*) system. Note that $\Delta\Phi_{bond} + \Delta\Phi_{bend} + \Delta\Phi_{Ag} \simeq \Phi - \Phi_0$ by definition.

DFT	Ag(110) (eV)	Ag(100) (eV)	Ag(111) (eV)
Φ_0	4.05	4.23	4.40
Φ	4.23	4.49	4.70
$\Phi - \Phi_0$	0.18	0.26	0.30
$\Delta\Phi_{bond}$	0.52	0.46	0.51
$\Delta\Phi_{bend}$	-0.35	-0.23	-0.17
$\Delta\Phi_{Ag}$	0.01	0.04	-0.03

change of the work function $\Delta\Phi_{bond}$ due to electron density redistributions (pushback effect and charge transfer). In all three cases, charge is transferred from the metal to the molecule. The ensuing bond dipole tends to increase the work function. The effect is of similar size for BW/Ag(110) and HB/Ag(111), and slightly smaller for T/Ag(100). For BW/Ag(110) the origin of the bond dipole is illustrated schematically in Fig. 8, where the laterally averaged adsorption-induced charge rearrangement is shown, as calculated with DFT. One clearly sees signatures of both the pushback effect (charge depletion of the metallic spill out in the plane of the molecule, by σ bonds, and below the molecule, by the π-lobes of the total electron density) and the charge transfer into the LUMO (charge accumulation in the π-lobes of the LUMO, both below and above the molecular plane). Twofold integration of this charge rearrangement over z yields the electrostatic potential, which shows a step through the PTCDA layer. This step $\Delta\Phi_{bond}$ corresponds to the bond dipole[54].

Since the sizes of the bond dipoles are determined by the combined action of three factors (amount of charge transfer, adsorption height, areal density of molecules), it is difficult to predict $\Delta\Phi_{bond}$ by inspection. BW/Ag(110) has the strongest charge redistribution, while HB/Ag(111) exhibits the highest areal density and the largest adsorption distance[23]. Apparently, the larger adsorption height and areal density for HB/Ag(111) together balance out the larger charge redistribution for BW/Ag(110), such that the $\Delta\Phi_{bond}$ in these two cases are similar. For T/Ag(100) the areal density is lower than for HB/Ag(111) at a similar adsorption height, and there is less charge redistribution than for BW/Ag(110). Together, this leads to a slightly lower bond dipole for T/Ag(100).

Secondly, the work function is changed by the dipole mo-

ment of the adsorbed molecule. In the present case this dipole is exclusively due to adsorption-induced bending of the molecule. For the associated $\Delta\Phi_{\mathrm{bend}}$ the situation can indeed be clearly related to structural distortions of the molecule: The distortion of PTCDA increases from HB/Ag(111) via T/Ag(100) to BW/Ag(110), and so does the bend dipole and hence $\Delta\Phi_{\mathrm{bend}}$. For BW/Ag(110) $\Delta\Phi_{\mathrm{bend}}$ is indicated in Fig. 8b. Note that it has opposite sign compared to $\Delta\Phi_{\mathrm{bond}}$, because the distortion is such that the negative partial charges on the carboxylic oxygen atoms move closer to the surface. The opposite orientations of the bond and bend dipoles can be seen by comparing Fig. 8 a and b.

Taking $\Delta\Phi_{\mathrm{bond}}$ and $\Delta\Phi_{\mathrm{bend}}$ together, the increase of the work function is largest for HB/Ag(111) and smallest for BW/Ag(110), thus the spread of the work functions of the three Ag surfaces is increased by PTCDA adsorption. In comparison to the work function changes directly related to the molecule ($\Delta\Phi_{\mathrm{bend}}$ and $\Delta\Phi_{\mathrm{bond}}$), the changes due to substrate surface buckling, which determine $\Delta\Phi_{\mathrm{Ag}}$, are neglegible (Table 3).

4.6 Electronic structure: The questions

In sections 4.3 and 4.4 we have seen that both adsorption height and energy level alignment are subject to complex processes at the interface. In the following we analyse how, despite these complexities, both quantities appear correlated, as observed in section 4.2 and Fig. 4. In particular, we ask two questions:

- Is there a way in which we could associate the frontier electronic structure of the molecules at the interface directly to an adsorbate-substrate bonding strength?
- How is the electronic structure of the frontier orbitals related to pertinent structural properties of the interface, most notably the adsorption height?

Regarding the first question we have to define what precisely is meant by adsorbate-substrate bonding strength. Large molecules like PTCDA interact with metals via different mechanisms: Next to the van der Waals interaction, there may be local chemical bonds between reactive atoms (such as the carboxylic oxygen atoms in PTCDA) and the substrate. Finally, there is the interaction between the extended π-electron system and the metal. Evidently, the van der Waals interaction is not relevant in the context of the above question, because it does not change the electronic structure of the adsorbate and it exhibits only a weak dependence on the substrate orientation, mainly via the adsorption height. Since local covalent bonds tend to involve molecular states with larger binding energies, their influence on the electronic structure in the energy region of the frontier orbitals is also small. However, we can anticipate that any chemical interaction of the molecular π-electron system with the metal will affect the frontier electronic structure. Therefore, one may ask whether the latter can be related to the adsorbate-substrate bonding strength *in this interaction channel*. In the following discussion, the term bonding strength therefore refers to the strength of the chemical interaction between the molecular π-system and the metal. We will refer to this as 'π–metal interaction' or 'π–metal bonding'.

Before addressing the above questions, we turn to an analysis of the experimentally observed energy level alignments of HOMO and LUMO at the three surfaces. This will offer first insights into the answer to question one.

4.7 Energy level alignments of HOMO and LUMO

Using the experimental data displayed in Fig. 3 and Table 2 in conjunction with the theoretical work function data discussed in section 4.5 (Table 3), we now analyse the energy level alignments of HOMO and LUMO relative the vacuum levels $E^{hkl}_{\mathrm{vac},0}$ and E^{hkl}_{vac} of the three bare and adsorbate-covered surfaces. It turns out that there are subtle differences in the behaviour of HOMO and LUMO, in spite of the superficial appearance of a nearly rigid shift relative to the Fermi level visible in Fig. 3.

However, before looking at this data, we construct the expected energy level alignment, using PTCDA gas phase and bulk data from the literature. The result is displayed in the centre of Fig. 9, in comparison with the actual alignment for HB/Ag(111) (left) and the gas phase (right). While this construction places the HOMO within 0.5 eV of the experimental binding energy (measured against E_{F}), the LUMO is found 1.7 eV *above* the Fermi level. Now it is well-known that upon adsorption at a metal surface the HOMO-LUMO gap as measured in photoelectron spectroscopy and inverse photoelectron spectroscopy will be reduced from the value for the bulk, due to screening effects of the charged final states, similar to what is observed in the transition from the gas to the condensed phase (cf. Fig. 9 right and middle). This moves both the HOMO and the LUMO closer to the Fermi level than predicted by the construction in Fig. 9. However, one would expect the screening to affect HOMO and LUMO roughly symmetrically, at variance with what is observed. While the effect on the HOMO is of the order 0.5 eV, the LUMO experiences a massive stabilization by almost 2 eV. This is an indication that HOMO and LUMO are implicated in the surface bonding in different degrees. We will come back to this in the context of bond stabilization in section 4.7.3.

4.7.1 HOMO In Fig. 10a the orbital binding energies of the HOMO are plotted in a scheme in which the vacuum levels of the three bare surfaces $E^{hkl}_{\mathrm{vac},0}$ are aligned. Remarkably, this reveals that the hypothetical ionization energies

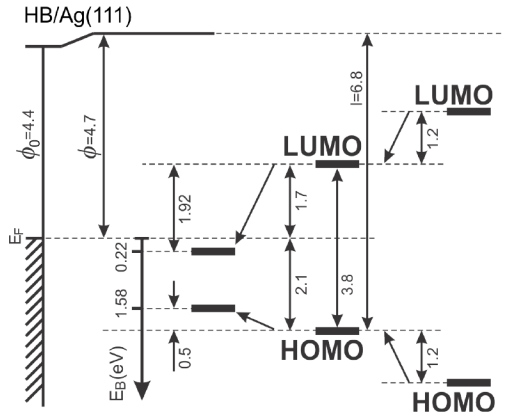

Fig. 9 Energy level alignment of HOMO and LUMO for HB/Ag(111). Right: gas phase PTCDA, left: experimentally observed alignment on Ag(111) (this work, Fig. 3 and Table 3). The expected level scheme of (bulk) PTCDA in contact with Ag(111) (middle) has been constructed from interface dipoles $\Phi^{hkl} - \Phi_0^{hkl}$ (this work), the bulk ionisation energy of PTCDA [60,83] and its bulk energy gap [61,84]. The gas phase scheme (right) has been constructed by adding (subtracting) 1.2 eV to the ionization potential (from the electron affinity), to account for the polarization in the bulk state. The value for the polarization has been taken from references [85,86].

$I_0 = E_B^{\mathrm{HOMO},hkl} + \Phi_0^{hkl}$ of the adsorbed PTCDA are identical ($I_0 \approx 5.95$ eV) for all three Ag surfaces to within 55 meV, in spite of HOMO binding energies (measured with respect to the Fermi level) ranging from 1.58 to 1.93 eV (spread 350 meV). This essentially means that different HOMO binding energies $E_B^{\mathrm{HOMO},hkl}$ on the three metal surfaces are precisely offset by different bare metal work functions Φ_0^{hkl}. Note that I_0 differs from the ionisation energy of the molecule in the bulk, which according to Fig. 9 is approximately 6.8 eV. The behaviour of the HOMO in Fig. 10a corresponds to vacuum level pinning with $S_0^{\mathrm{HOMO}} = dE_B^{\mathrm{HOMO}}/d\Phi_0 \simeq -1$ (Note that the index 0 denotes the fact that S is evaluated for the vacuum level of the bare surface).

The finding of Fig. 10a would therefore suggest a weak interaction of the PTCDA HOMO with the metal. In particular, the ionization energy of the adsorbate is affected only unspecifically (i.e., in the same way on all three surfaces) by the adsorption. This is surprising, since charge transfer from the metal to the molecule and molecular distortions are all different on the three surfaces and could therefore influence the ionization energy differently. Moreover, also the final state effect of core hole screening after photo-ionization of the HOMO may be expected to be surface-specific, as smaller adsorption heights should favour screening and thus reduce the ionization energy. Finally, for the relevant molecule-surface adsorption distances, the electrostatic potential in front of the surface itself varies rapidly as a function of z. Hence, the adsorption height should influence the ionization energy (smaller adsorption height should lead to an increase of I). The remarkable finding then is that in the end all of these factors conspire to emulate a hypothetical weak-interaction situation across all surfaces: *One* universal hypothetical ionization energy I_0 (hypothetical because referenced to Φ_0^{hkl}) is sufficient to largely explain the *true* line-up of the HOMO with respect to the Fermi level on all three surfaces.

4.7.2 LUMO A close view at Table 2 reveals that the LUMO binding energy increases in the sequence HB/Ag(111) $\rightarrow$ T/Ag(100) $\rightarrow$ BW/Ag(110) more rapidly than the HOMO binding energy. Since in the same sequence $\Delta\Phi = \Phi - \Phi_0$ decreases, we have plotted in Fig. 10b level positions aligned at the vacuum levels of the molecule-covered surfaces E_{vac}^{hkl}, and indeed we find that $I' = E_B^{\mathrm{LUMO},hkl} + \Phi^{hkl}$ is nearly identical for all three surfaces ($I' \approx 4.95$ eV), within 65 meV, in spite of LUMO binding energies (measured with respect to the Fermi level) ranging from 0.215 to 0.75 eV (spread 535 meV).

I' corresponds to the ionization potential of the occupied LUMO. Thus, Fig. 10b shows that the ionization energy from the filled LUMO is largely independent of the substrate surface on which PTCDA is adsorbed (it should be noted here that I' is not strictly related to the electron affinity E_A of the neutral molecule, which according to Fig. 9 is $\simeq$ 3 eV). The near identity of the ionization energies I' from the LUMO for different surfaces is remarkable, because the different amounts of charge transfer, different adsorption heights and ensuing different degrees of hybridisation and charge reorganization, and the different molecular distortions all have an influence on the orbital. Yet, this is what is observed, and this indicates that as far as removing an electron from the filled LUMO into the vacuum is concerned, there does not appear to be too much difference between the three surfaces. Accordingly, for the negatively charged molecule we observe approximate pinning of the LUMO to the vacuum level of the PTCDA-covered surface, $S^{\mathrm{LUMO}} = dE_B^{\mathrm{LUMO}}/d\Phi \simeq -1.1$. In other words, the LUMO seems related to Φ as the HOMO is related to Φ_0.

4.7.3 Bond stabilization of the LUMO Looking at Fig. 10, we see that depending on whether alignment at E_{vac}^{hkl} (right) or $E_{\mathrm{vac},0}^{hkl}$ (left) is considered, the HOMO either partially follows the Fermi level or stays pinned to the vacuum level. In other words, its S-parameter is always larger than -1 ($S^{\mathrm{HOMO}} \simeq -0.7 > -1$) or equal to -1 ($S_0^{\mathrm{HOMO}} \simeq -1$). On the other hand, the LUMO shifts in the *opposite* direction than the Fermi level as the work function is decreased. While this effect is small for alignment at E_{vac}^{hkl} ($S^{\mathrm{LUMO}} \simeq -1.1$), it is substantial for alignment at E_{vac}^{hkl}, leading to a value of $S_0^{\mathrm{LUMO}} \simeq -1.5 < -1$. In the language of the IDIS model, this corresponds to a situation in which the effect of the work function on the binding energy of the level is amplified instead of screened. Such a behaviour lies outside the bounds of the IDIS

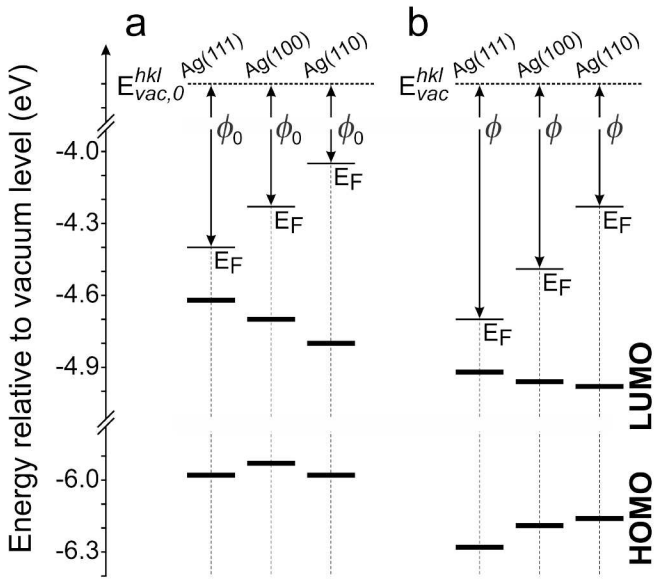

Fig. 10 HOMO and LUMO positions in PTCDA monolayers on Ag(111), Ag(100) and Ag(110). Binding energy data are taken from Table 2, work function data from Table 3. (a) Vacuum levels of the bare surfaces $E^{hkl}_{\mathrm{vac},0}$ are aligned. (b) Vacuum levels of the molecule covered surfaces E^{hkl}_{vac} are aligned.

model.

Hence, there must be an additional mechanism beyond that of the IDIS model that influences the LUMO binding energies when switching between the different substrate surface orientations. We suggest this to be *bond stabilization*: It is a well-known effect that orbitals which are implicated in the chemical bonding of a molecule to a surface move to higher binding energies, i.e. are stabilized relative to other orbitals by their participation in the bonding[87]. Note that the Fermi level rather than the vacuum level is the correct reference energy for bond stabilization, since the electron needs only be lifted to the level of the lowest unoccupied states of the system, i.e., just above the Fermi level, to escape from the state in question and thus break the bond.

At this point we turn back to Fig. 9, which, as we have discussed at the beginning of the current section, indicates a massive bond stabilization of the LUMO relative to the HOMO on *all* three surfaces. In the light of this, the observed behaviour of the LUMO in Fig. 10a indicates a *differential* bond stabilization of the LUMO, i.e. a bond stabilization that increases in the sequence $(111) \rightarrow (100) \rightarrow (110)$, in addition to the overall bond stabilization found on all Ag surfaces. This reveals an increasing strength of chemical π–metal bonding of PTCDA in the same sequence, as also suggested by, e.g., adsorption heights. Moreover, the observation that only the LUMO shows an S-parameter $S < -1$, while the HOMO's S-parameters are found in the range between 0 and -1, indicates that of the two frontier orbitals the LUMO is more strongly involved in surface bonding.

4.8 Relation between orbital binding energies, π–metal bonding strengths and adsorption heights

The different behaviours of HOMO and LUMO show clearly that primarily the latter is involved in the π–metal interaction of the molecule to the surface. We now finally turn to the two questions which we have posed before: In which way is the electronic structure, most notably the orbital binding energies of the relevant frontier orbitals, related to the chemical π–metal bonding strength and the adsorption height? To approach these questions we employ the canoncial Newns-Anderson (NA) model of chemisorption for a conceptual discussion of the interaction between the LUMO of PTCDA and the three Ag surfaces. As we will see, the NA model allows a surprisingly realistic estimate of the π–metal chemisorption energy for PTCDA/Ag.

4.8.1 Chemical bonding strength due to π–metal interaction

4.8.1.1 The model Hamiltonian The NA model is a generic model to understand the basic phenomenology of chemical adsorption. Newns[88] adapted Anderson's model Hamiltonian[89], which was originally introduced to describe magnetic impurities in metals, to the problem of the chemical interaction of an adsorbate with a metal surface. In the NA model, the adsorbate and the metal surface are represented by a single local orbital at energy ε_{a} and a single band $\varepsilon_{\mathbf{k}\sigma}$, respectively. The interaction between the two is captured by hybridisation matrix elements $V_{\mathbf{k}\sigma}$. Furthermore, it is essential to take the electron-electron interaction within the local orbital into account. To this end, a parameter U that quantifies the Coulomb repulsion between two electrons in the local orbital is introduced: While the first electron in the local orbital has a binding energy ε_{a}, the second one has the binding energy $\varepsilon_{\mathrm{a}} + U$. The two-particle interaction term $U n_{-\sigma} n_{\sigma}$, where n_{σ} is the number of electrons with spin σ in the local orbital, complicates the solution of the NA model considerably. For this reason, Newns introduced the Hartree-Fock (HF) approximation, in which the two-particle interaction is replaced by $U\langle n_{-\sigma}\rangle n_{\sigma}$, where $\langle n_{-\sigma}\rangle$ is the average occupancy of the local level with electrons of spin $-\sigma$. This leads to two coupled Hamiltonians, one for each spin σ, in which the energy of the local orbital becomes $\varepsilon_{\sigma} = \varepsilon_{\mathrm{a}} + \langle n_{-\sigma}\rangle U$. A full discussion of the HF solution of this classical problem is given in the original paper by Newns[88] and in many other sources[90,91]. Here we focus on those aspects which are relevant in the present context.

4.8.1.2 Classification of possible solutions. There are several types of solutions of the NA Hamiltonian which can best

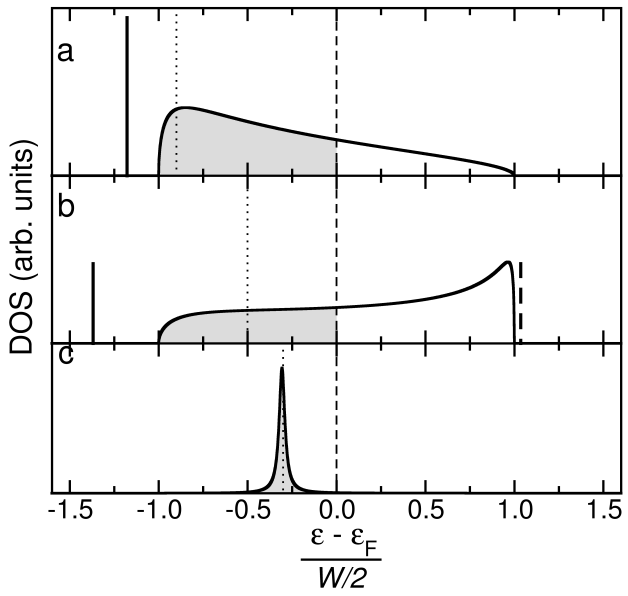

Fig. 11 Spectral functions of solutions of the Newns-Anderson model ($U = 0$, semi-infinite one-dimensional chain, nearest-neighbour interaction only). (a) A single localized state below the band (parameters: $V = 0.5$, $\varepsilon_F = 0$, $\varepsilon_a = -0.9$). (b) A pair of localized states, one below the band, the other above ($V = 1.0$, $\varepsilon_F = 0$, $\varepsilon_a = -0.5$). (c) A resonance in the occupied part of the band ($V = 0.1$, $\varepsilon_F = 0$, $\varepsilon_a = -0.3$). All energies are expressed in units of $W/2$. Note that in the three panels the DOS-scale is different. Chemisorption energies are: (a) $\Delta E = -2.0$, (b) $\Delta E = -2.1$, (c) $\Delta E = -0.62$. Note that in all cases $\Delta E < -2\varepsilon_a$. The deviation from $-2\varepsilon_a$ is due to the perturbation of states in the metal band (level repulsion away from the local state/resonance), expressed through the integral in equation (4).

be visualized in energy level diagrams such as in Fig. 11. The diagrams were drawn on the basis of a HF solution of the NA Hamiltonian under the assumption of a tight binding band derived for a semi-infinite one-dimensional chain, interacting at its 'surface' with a local orbital; in spite of its simplicity, this 1D model captures the physical phenomenology well.

The different types of solutions are: (a) One single localized state appears, either above the upper band edge or below the lower band edge of the metal (Fig. 11a). (b) A pair of local states appears, one above, the other below the metal band (Fig. 11b). (c) No truly local state but a local resonance in the metal band appears; electrons in this resonance have a finite life time, since they can transfer to the metal band and thus escape into the metal (Fig. 11c). Situation (a) prevails for ε_σ outside the band, or for intermediate hybridization when ε_σ is inside the band but close to the band edge. Situation (b) is found for large hybridisation $V \gg W$, where W is the width of the metal band, and it corresponds to the splitting of the local orbital ε_σ into a bonding and an anti-bonding state, similar to what is observed for chemical bond formation between atoms. This situation is often discussed in the context of interaction with a *d*-band (strong chemisorption). Finally, situation (c) occurs if the level ε_σ is located inside the metallic band, reasonably far from the band edges, and the hybridisation is weak ($V \ll W$, weak chemisorption). Situation (c) is the situation which we encounter in the case of PTCDA adsorption on Ag surfaces, if we identify the local level ε_σ with the LUMO of PTCDA. Indeed, we observe in experiment that the LUMO with binding energies between 0.3 and 0.9 eV below the Fermi level is degenerate with the *sp*-band of Ag, it is only slightly broadened into a resonance (the typical FWHM in Fig. 3 is 0.5 eV, compared to a *sp*-band width W of the order 10 eV), and there are no signs of it splitting into a bonding and an anti-bonding state.

4.8.1.3 Initial position of the local level. Next we have to address the issue of the local level's position on the energy axis. The relevant level positions *before* hybridisation are the ε_σ. However, because of the existence of U these level positions ε_σ depend on the occupancy of the level with electrons of opposite spin $-\sigma$. This occupancy can be calculated from the spectral function $\rho_\sigma(\varepsilon)$ of the local level *after* hybridisation. The HF approximation of the NA Hamiltonian therefore requires a self-consistent solution. Mostly one is interested in non-magnetic solutions for which $\langle n_{-\sigma}\rangle = \langle n_\sigma\rangle$. While such solutions always exist, they are not always the ones with the lowest energy (if magnetic solutions exist, they have lower energy[89]). Only if the Coulomb repulsion $U \approx 0$ can we use the bare level energy ε_a as an input for the solution of the hybridisation problem. This has been done in Fig. 11.

The position of the bare level ε_a is, far away from the surface, determined by the alignment of the vacuum levels of the

bare surface and the gas phase molecule, as discussed above. But if, as is the case in the present system, the LUMO finally ends up below the Fermi level, the level energy ε_a will be stabilized by the electrostatic attraction between the charged molecule and the induced image dipole in the metal surface. The affinity level ε_a of the initially isolated molecule will thus follow the one-electron image potential as the molecule approaches the surface[90]. Hence, the position of ε_a on the energy axis is determined by the electron affinity of the isolated molecule (vacuum level alignment) plus the image charge attraction.

4.8.1.4 Chemisorption energy. In the literature, the chemical binding energy in the NA model is less often discussed than the resultant density of states. But, of course, within its bounds the model allows a precise calculation of the chemisorption energy[88]. In the NA model, the chemisorption energy is given by[88]

$$\Delta E = \left[\sum_{m\sigma,\mathrm{occ.}} \varepsilon_{m\sigma} - U\langle n_\sigma\rangle\langle n_{-\sigma}\rangle\right] - \left[2\sum_{\mathbf{k},\mathrm{occ.}} \varepsilon_{\mathbf{k}\sigma} + f\left[\varepsilon_a + (f-1)\frac{U}{2}\right]\right]. \quad (2)$$

The first term is the total energy of the perturbed (i.e. hybridized) system (quantum numbers m and σ summed over all occupied states), while the last term gives the total energy of the non-interacting system, where we assume that the local level is initially either empty ($f = 0$), singly ($f = 1$) or doubly occupied ($f = 2$); for the LUMO (HOMO) $f = 0$ ($f = 2$), respectively. In the first sum the term $U\langle n_\sigma\rangle\langle n_{-\sigma}\rangle$ is subtracted to avoid double counting, because in the $\varepsilon_{m\sigma}$ this term is contained twice. The above equation can be expressed more compactly as[88]

$$\Delta E = \sum_\sigma \Delta E^{1\sigma} - U\langle n_\sigma\rangle\langle n_{-\sigma}\rangle - f\left[\varepsilon_a + (f-1)\frac{U}{2}\right] \quad (3)$$

where $\Delta E^{1\sigma}$ is the difference between occupied one-particle energies of the perturbed and unperturbed systems. This expression can be evaluated, using the calculus of residues in the complex plane, to yield[88]

$$\Delta E^{1\sigma} = \varepsilon_{1\sigma} - \varepsilon_0 + \sum_\sigma \frac{1}{\pi}\int_{\varepsilon_0}^{0} \tan^{-1}\frac{\Delta(\varepsilon)}{\varepsilon - \varepsilon_\sigma - \Lambda(\varepsilon)} d\varepsilon \quad (4)$$

where ε_0 is the bottom of the band (the integration is carried out up to the Fermi level which is set to zero) and $\Delta(\varepsilon)$ is a hybridisation-weighted density of states function and $\Lambda(\varepsilon)$ its Hilbert transform. Equation (4) shows that there are two contributions to the energy change on chemisorption: Firstly, if a localized state $\varepsilon_{1\sigma}$ splits off from the bottom of the band, this will lead to an energy gain of $\varepsilon_{1\sigma} - \varepsilon_0$ per spin. Secondly,

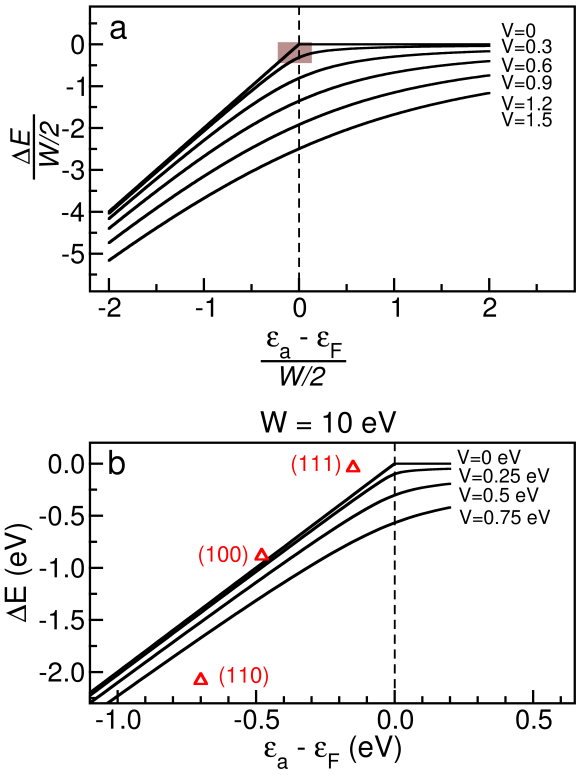

Fig. 12 (a) Chemisorption energy of a single orbital calculated within the framework of the Newns-Anderson model ($U = 0$, semi-infinite one-dimensional chain, nearest-neighbour interaction only), as a function of unperturbed level position ε_a, for various hybridisation parameters V in the range $V = 0$ to $V = 1.5$ in steps of 0.3. Hybridisation parameters below $V \simeq 0.7$ (for $\varepsilon_a = 0$) correspond to solutions of type (c) in Fig. 11 (local resonance). All energies are expressed in units of $W/2$. The grey rectangle indicates the parameter region of the zoom in panel b. (b) Zoom into the diagram of panel a, with axes in absolute energies. W =10 eV has been used as a rough estimate for the width of the Ag *sp*-band. Red triangles show the chemisorption energies of DFT-GGA calculations for HB/Ag(111), T/Ag(100) and BW/Ag(110), in which the adsorption heights of the carbon backbones have been fixed to the experimental heights, whereas the positions of the remaining atoms are relaxed. The ε_a values are taken from the PDOS-LUMO peak positions in Fig. 7. Chemisorption energies are: HB/Ag(111): -0.04 eV, T/Ag(100): -0.87 eV, BW/Ag(110): -2.08 eV. For comparison, the total binding energies including van der Waals are: HB/Ag(111): -4.13 eV, T/Ag(100): -4.83 eV, BW/Ag(110): -5.71 eV. Note that as expected the van der Waals binding energy decreases slightly with increasing openness of the surface: HB/Ag(111): -4.09 eV, T/Ag(100): -3.96 eV, BW/Ag(110): -3.63 eV.

all metal levels will slightly be perturbed, in such a way that each new eigenvalue $\varepsilon_{m\sigma}$ is bounded by two old ones $\varepsilon_{\mathbf{k}\sigma}$, one above and one below (interpolative property of the perturbed solution), leading to an overall energy change that is expressed by the integral in equation (4) .

The integral in equation (4) can by evaluated analytically for the case of a 1D tight binding band, which yields a semi-elliptic $|V_{\mathbf{ak}}|^2$-weighted density of states $\Delta(\varepsilon)$. We discuss the results of this evaluation for the initially empty LUMO ($f = 0$). Disregarding U for simplicity, i.e. $\varepsilon_\sigma = \varepsilon_a$, chemisorption energies are plotted in Fig. 12a as a function of the initial LUMO position ε_a for a range of different hybridisation parameters $V_{\mathbf{ak}}$. One clearly sees that for positions ε_a below the Fermi level, the (one-electron) chemisorption energy $|\Delta E|$ rises with the unperturbed binding energy ε_a of the LUMO.

The explanation of this behaviour is straightforward: As ε_a moves below the Fermi level, two electrons can drop from the Fermi level into the initially empty LUMO. This is seen very clearly in the limit of $V_{\mathbf{ak}} \to 0$, whence the chemisorption energy becomes just twice the binding energy of the LUMO (Fig. 12a). For non-zero $V_{\mathbf{ak}}$ the chemisorption energy $|\Delta E|$ at a given level position ε_a increases from $|2\varepsilon_a|$. The reason is that all metal states below the resonance are pushed down ever so slightly. In sum, this yields an appreciable contribution to the chemisorption energy. It is evident from Fig. 12a that this effect is largest for LUMO positions ε_a close to the Fermi level, because by level repulsion all metal states *below* the resonance are pushed down, and this means that as the resonance moves deeper into the occupied part of the band, the bonding contribution of the metal states as a whole decreases, as a *decreasing* number of metal states are pushed *down* and an *increasing* number are pushed *up*. However, Fig. 12a unambiguously shows that in the parameter range that we are interested in, in which the LUMO survives as a well-defined resonance, the link in the NA model between the binding energy of the LUMO and the chemisorption energy of adsorbate remains valid. In particular, the fully occupied LUMO resonance remains bonding at all positions below the Fermi level. Fig. 12a also reveals that in the case of non-zero hybridisation there is a non-zero chemisorption energy even if ε_a is located *above* the Fermi level. On the one hand, this is again a consequence of level repulsion (in this case all occupied metal states are lowered in energy), and on the other hand the broadening of the LUMO means that part of its density of states becomes occupied even before the peak moves below the Fermi level.

In Fig. 12a it is evident that the non-perturbed level position ε_a of the LUMO determines the chemisorption energy. But, of course, this initial level position is experimentally not accessible, since we only know the position of the resonance of the perturbed system. However, turning to Fig. 11, we observe that as long as resonance is clearly observed (small hybridisation) the shift of the resonance away from ε_a is small. Hence

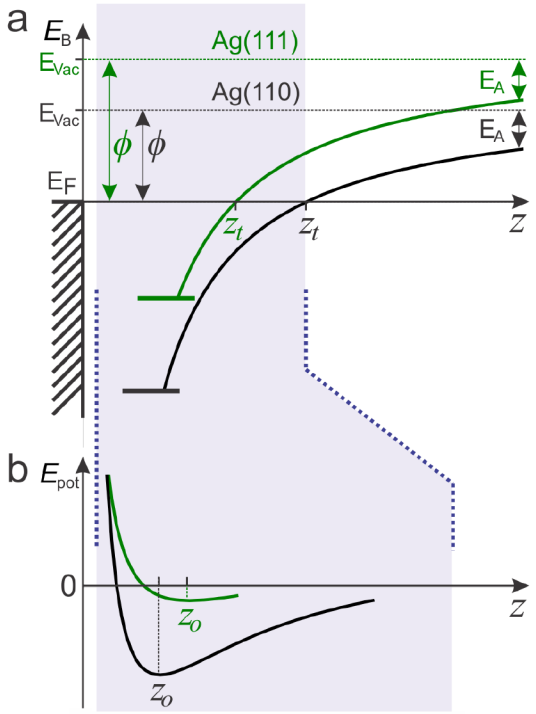

Fig. 13 Schematic view of LUMO binding energy alignment, molecular adsorption height and π–metal bonding strength in the Newns-Anderson model (not to scale). (a) The LUMO level of the molecule follows the one-electron image potential in front of the surface. This is shown for a high-work function metal (green, e.g. Ag(111)) and a low work function metal (black, e.g. Ag(110)). (b) The sum of attractive and repulsive energies shows stronger bonding and shorter adsorption height for the low-work function metal, which also has the larger LUMO binding energy (panel a). For a more detailed discussion, cf. text.

we can roughly read off the non-perturbed ε_a from the experimental LUMO position.

In Fig. 12b we have replotted Fig. 12a on an absolute energy scale, estimating the Ag *sp*-band width as $W = 10\,eV$. To compare the chemisorption energies calculated according to equation (4) in the one-dimensional tight binding case to the chemisorption energies of the PTCDA/Ag system, we have added the results of DFT-GGA calculations for HB/Ag(111), T/Ag(110) and BW/Ag(110) to Fig. 12b. Note that the plotted energies exclude the contributions of the van der Waals interaction, since we are interested in the chemical component of the PTCDA/Ag interaction only. Because neglecting the van der Waals interaction usually results in too large adsortion distances for highly polarizable π-conjugated molecules on metal surfaces, we have in these calculations fixed the PTCDA carbon backbones to the experimental positions (4). In this way, one expects a realistic result for the chemisorption energies.

Fig. 12b shows that the NA model reproduces the trend observed for the chemisorption energies of PTCDA on the three Ag surfaces remarkably well. In particular, the correlation between the LUMO binding energies ε_a and the chemisorption energies is also present in the DFT calculation. The fact that this correlation is steeper in the case of the DFT is expected, because the DFT calculations, in which relaxtions of the oxygen (and hydrogen) positions are allowed, also include the contributions of local bonds to the chemisorption energies, and we know from the increasing distortion of PTCDA that these get stronger in the sequence (111)→(100)→(110)[23]. We can thus conclude that in spite of its simplicity the NA model does predict the trend of the chemisorption energies for PTCDA on the three Ag surfaces correctly. The insight into the bonding mechanism offered by this simple model calculation can therefore be transfered to the PTCDA/Ag system. In essence, this means that the chemisorption energy of the π-system of PTCDA on Ag surfaces can be approximatively read off from the LUMO binding energy, as predicted by the NA model.

4.8.2 Adsorption height Finally, we consider a *gedankenexperiment* which helps us to establish a connection between the LUMO binding energy, the chemisorption energy of the π-system and the adsorption height[58]. Imagine that the molecule approaches the surface from far away. As discussed above, the molecular vacuum level rides on the potential outside the metal surface (vacuum level alignment). At large distances between molecule and surface there is only the van der Waals attraction between the two, which has no bearing on the present argument. Also, we assume that hybridization is weak, such that the LUMO orbital is essentially unperturbed.

As the molecule approaches the surface, the affinity level E^A (LUMO) moves down (Fig. 13), because of image charge stabilization, although the affinity level is still empty[90]. At the position z_t when E^A aligns with the Fermi level of the metal, an electron can be moved from the metal to the molecule at no energy cost. Once this electron has been moved, the molecule is charged, and there will be a real attraction between molecule and metal. When moving the charged molecule closer to the metal, energy is released until the molecule reaches its equilibrium position z_0 above the surface. The energy released up to z_0, which in this *gedankenexperiment* is the chemisorption energy, can be calculated as the integral over the force along the path. The further away z_t is from z_0, the larger is the chemisorption energy, because the distance range $z_t - z_0$ over which the otherwise identical image force is integrated is longer. According to Fig. 13a the point z_t will be determined by the electron affinity of the molecule and the work function of the metal.

Three things should be noted: First, in this *gedankenexperiment* the bond stabilization of the LUMO that was discussed earlier is primarily effected by the image charge attraction (Fig. 13a). Secondly, the *gedankenexperiment* recovers the result of the NA model (for negligible hybridisation), namely that the chemisorption energy corresponds to the LUMO binding energy relative to the Fermi level. Thirdly, as Fig. 13b shows, while an earlier onset of the charge transfer will lead to a deeper potential well of the sum potential between attractive (image charge) and repulsive (Pauli repulsion) branches, it will in itself not necessarily lead to a shorter bond length, and thus also not to a differential bond stabilization of the LUMO for surfaces with lower z_0. However, if it is taken into account that a smaller work function, which in the first place leads to an earlier charge transfer (i.e. larger z_t, see Fig. 13a), also implies a later onset of Pauli repulsion, it becomes clear that the deeper potential will also have its minimum at shorter adsorption distance z_0 and hence will yield a differential bond stabilization of the LUMO (Fig. 13b). Thus, a larger LUMO binding energy not only indicates a stronger π–metal chemical bonding, but it also correlates with a smaller adsorption distance.

5 Conclusion

We have presented a systematic analysis of the electronic structure of PTCDA monolayers on Ag surfaces, with special emphasis on the link to the geometric interface structure. This has been achieved by comparing the molecular level alignments for the three canonical low index surface orientations of Ag, on which PTCDA forms structurally distinct monolayers. In particular, we have discussed the connection between molecular adsorption height, orbital binding energies and π–metal bonding strength, i.e. the strength of the chemical bond between the molecular π-system and the metal. The conceptual discussion, employing experimental data, first- principles calculations and a generic model, has allowed the rationaliza-

tion of the essential experimental observations for the system under study. It is anticipated that many of the results have validity beyond this specific material system. However, we stress that the analysis presented here is limited to adsorbates whose chemical interaction with the substrate is weak. For more strongly interacting systems the behaviour is expected to differ substantially. For example, the current analysis disregards the contribution from *d*-bands completely. For Ag surfaces this is justified, because of the relatively deep-lying *d*-bands. For Cu, on the other hand, the *d*-bands may well play a more prominent role.

We also note again that the π–metal interaction on which we have focussed here because it is directly connected to the energy level alignment of frontier orbitals (after all, these are π-orbitals) is only one of several interaction types with which the PTCDA molecule interacts with the Ag substrate. The interaction of the molecule with the surface furthermore includes the van der Waals interaction as well as contributions from local chemical bonds between the carboxylic oxygen atoms and the substrate. In fact, the largest contribution to the overall adsorption energy is the due to the van der Waals interaction, and the local chemical bonds have been dicussed extensively in references[23,57]. Since in ab initio calculations it is difficult to partition the total chemical interaction into contributions due to the π–metal interaction and the local bonds, it is an interesting finding of the present work that in the weak chemisorption limit the π–metal bonding can be extrapolated from the relevant experimental orbital binding energies.

Our analysis has shown that for PTCDA on Ag surfaces the LUMO plays a pivotal role in the π–metal interaction, while the HOMO is rather more passive. In particular, we find that at the interface the LUMO of PTCDA is subject to massive bond stabilization, and that this varies between the different interfaces which we have studied in a way that cannot be accounted for in the common model of energy level alignment at metal-organic interfaces, i.e. the model based on an induced density of interface states (IDIS). The behaviour of the HOMO, incidentally, can be explained on the basis of the IDIS model. The Newns-Anderson model of chemisorption reveals that the orbital binding energy of the LUMO scales with the π–metal chemisorption energy, because the latter is to a large extent determined by the energy gain due to the charge transfer of electrons from the Fermi level of the metal into the stabilized LUMO. Within the same model we can also identify a causal link between the differential bond stabilization of the LUMO and the adsorption height. This means that the overall adsorption height of PTCDA on Ag surfaces is primarily determined by the interaction of the molecular π-system with the metal, not by the functional groups. The local bonds lead to a vertical distortion of the molecule, but they have only a minor influence on its overall adsorption height[92]. Finally, we have seen that the central property which controls a surface's reactivity towards an extended adsorbate (and thus quantities such as adsorption height, bond stabilization and chemical interaction strength) is the work function. It is interesting to note here that because of their generally small work functions (a global property) open surfaces, which due to their undercoordination (a local property) exhibit a large surface reactivity towards small adsorbates, do the same for extended adsorbates.

In summary, we have argued that for weakly chemisorbed π-conjugated molecules the here observed relationships between overall adsorption height, frontier orbital binding energies and π–metal bonding strength can be understood from very general principles and constitute the 'normal (canonical) case'. With hindsight, it is not surprising that these quantities are closely related, because all of them are connected to the molecular π-electron system. In this context it is noteworthy that in the case of heteromolecular hybrid interfaces, in which differerent molecular species (e.g. donor and acceptor molecules) form mixed monolayers on the metal substrate, this canonical relationship is broken, as has been discussed in detail elsewhere[22,93–95]. However, as has been shown in reference[22], the same concepts as developed here still apply to mixed monolayers, but due to a more complex situation the outcome is different.

6 Acknowledgements

The authors gratefully acknowledge valuable discussions with M. Sokolowski (University of Bonn).

References

1 S. Narioka, H. Ishii, D. Yoshimura, M. Sei, Y. Ouchi, K. Seki, S. Hasegawa, T. Miyazaki, Y. Harima and K. Yamashita, Appl. Phys. Lett. **67**, 1899 (1995).
2 I.G. Hill, A. Rajagopal, A. Kahn, Y. Hu, Appl. Phys. Lett. **73**, 662 (1998).
3 H. Ishii, K. Sugiyama, E. Ito and K. Seki, Adv. Mater. **11**, 605 (1999).
4 F. Baier, F. v Ludowig, A. Soukopp, C. Väterlein, J. Laubender, P. Bäuerle, M. Sokolowski, E. Umbach, Optical Materials **12**, 284 (1999).
5 Conjugated Polymer And Molecular Interfaces: Science And Technology For Photonic and Optoelectronic Applications, edited by W. R. Salaneck,K. Seki, A. Kahn, J.-J. Pireaux (Dekker, New York, 2002)
6 H. Peisert, M. Knupfer and J. Fink, Appl. Phys. Lett. **81**, 2400 (2002).
7 D. Cahen and A. Kahn, Adv. Mater. **15** 271 (2003).
8 D. Cahen, A. Kahn, E. Umbach, Mater. Today, **8**, 32 (2005).

9 H. Yamane, D. Yoshimura, E. Kawabe, R. Sumii, K. Kanai, Y. Ouchi, N. Ueno, and K. Seki, Phys. Rev. B **76**, 165436 (2007).

10 N. Koch, ChemPhysChem. **8** 1438 (2007).

11 N. Ueno and S. Kera, Prog. in Surf. Sci. **83**, 490 (2008).

12 J. D. Sau, J. B. Neaton, H. J. Choi, S. G. Louie, and M. L. Cohen, Phys. Rev. Lett. **101**, 026804 (2008).

13 S. Kera, H. Yamane, N. Ueno, Prog. in Surf. Science **84**, 135 (2009).

14 H. Yamane, A. Gerlach, S. Duhm, Y. Tanaka, T. Hosokai, Y. Y. Mi, J. Zegenhagen, N. Koch, K. Seki, and F. Schreiber, Phys. Rev. Lett. **105**, 046103 (2010).

15 L. Giovanelli, F. C. Bocquet, P. Amsalem, H.-L. Lee, M. Abel, S. Clair, M. Koudia, T. Faury, L. Petaccia, D. Topwal, E. Salomon, T. Angot, A. A. Cafolla, N. Koch, L. Porte, A. Goldoni, and J.-M. Themlin, Phys. Rev. B **87**, 035413 (2013).

16 J. Hwang, A. Wan, A. Kahn, Mat. Sci. Eng. R **64**, 1 (2009).

17 S. Braun, W. R. Salaneck and M. Fahlman, Advanc. Mater. **21**, 1450 (2005).

18 G. Witte and Ch. Wöll, J. of Mater. Res. **19**, 1889 (2004).

19 J. Götzen, D. Käfer, Ch. Wöll and G. Witte, Phys. Rev. B. **81**, 085440 (2010).

20 A. Gerlach, C. Bürker, T. Hosokai, and F. Schreiber, X-Ray standing waves and surfaces X-ray scattering studies of molecule-metal interface, in "The Molecule-Metal Interface" (edited by N. Koch, N. Ueno, A. T. S. Wee), John Wiley / VCH Weinheim (2013).

21 G. Heimel, S. Duhm, I. Salzmann, A. Gerlach, A. Strozecka, J. Niederhausen, C. Bürker, T. Hosokai, I. Fernandez-Torrente, G. Schulze, S. Winkler, A. Wilke, R. Schlesinger, J. Frisch, B. Bröker, A. Vollmer, B. Detlefs, J. Pflaum, S. Kera, K. J. Franke, N. Ueno, J. I. Pascual, F. Schreiber, N. Koch, Nat. Chemistry **5**, 187 (2013).

22 B. Stadtmüller, D. Lüftner, M. Willenbockel, E. M. Reinisch, T. Sueyoshi, G. Koller, S. Soubatch, M. G. Ramsey, P. Puschnig, F. S. Tautz, and C. Kumpf, Nat. Comm. **5** doi:10.1038/ncomms4685 (2014).

23 O. Bauer, G. Mercurio, M. Willenbockel, W. Reckien, C. H. Schmitz, B. Fiedler, S. Soubatch, T. Bredow, F. S. Tautz, M. Sokolowski, Phys. Rev. B **86**, 235431 (2012).

24 C. Seidel, C. Awater, X. D. Liu, R. Ellerbrake, H. Fuchs, Surf. Sci. **371**, 123 (1997).

25 K. Glöckler, C. Seidel, A. Soukopp, M. Sokolowski, E. Umbach, M. Böhringer, R. Berndt, W. D. Schneider, Surf. Sci. **405**, 1 (1998).

26 M. Böhringer, W. D. Schneider, K. Glöckler, E. Umbach, R. Berndt, Surf. Sci. **419**, L95 (1998).

27 M. Willenbockel, B. Stadtmüller, K. Schönauer, F. C. Bocquet, D. Lüftner, E. M. Reinisch, T. Ules, G. Koller, C. Kumpf, S. Soubatch, P. Puschnig, M. G. Ramsey, F. S. Tautz, New J. Phys. **15**, 033017 (2013).

28 M. Wießner, D. Hauschild D, A. Schöll, V. Feyer, K. Winkler, B. Krömker, F. Reinert F, Phys. Rev. B **86**, 045417 (2012).

29 C. Seidel, J. Poppensieker, H. Fuchs, Surf. Sci. **408**, 223 (1998).

30 D. Braun, A. Schirmeisen, H. Fuchs, Surf. Sci. **575**, 3 (2005).

31 J. Ikonomov, O. Bauer, M. Sokolowski, Surf. Sci. **602**, 2061 (2008).

32 L. Kilian, E. Umbach, M. Sokolowski, Surf. Sci. **573**, 359 (2004).

33 B. Stadtmüller, M. Willenbockel, E. M. Reinisch, T. Ules, F. C. Bocquet, S. Soubatch, P. Puschnig, G. Koller, M. G. Ramsey, F. S. Tautz, C. Kumpf, Euro Phys. Lett. **100**, 26008 (2012).

34 A. Kraft, R. Temirov, S. K. M. Henze, S. Soubatch, M. Rohlfing, F. S. Tautz, Phys. Rev. B **74**, 041402(R) (2006).

35 G. Koller, S. Berkebile, M. Oehzelt, P. Puschnig, C. Ambrosch-Draxl, F. P. Netzer, M. G. Ramsey, Science **317**, 351 (2007).

36 P. Puschnig, S. Berkebile, A. J. Fleming, G. Koller, K. Emtsev, T. Seyller, J. D. Riley, C. Ambrosch-Draxl, F. P. Netzer, M. G. Ramsey, Science **326**, 702 (2009).

37 J. Ziroff, F. Forster, A. Schöll, P. Puschnig, F. Reinert, Phys. Rev. Lett. **104**, 233004 (2010).

38 P. Puschnig, E. M. Reinisch, T. Ules, G. Koller, S. Soubatch, M. Ostler, L. Romaner, F. S. Tautz, C. Ambrosch-Draxl and M. G. Ramsey, Phys. Rev. B **84**, 235427 (2011).

39 L. Broekmann, A. Tadich, E. Huwald, J. Riley, R. Leckey, T. Seyller, K. Emtsev, L. Ley, J. Electron. Spectrosc. Relat. Phenom. **144-147**, 1001 (2005).

40 J. P. Perdew, K. Burke, and M. Ernzerhof, Phys. Rev. Lett. **77**, 3865 (1996).

41 X. Gonze, B. Amadon, P.-M. Anglade, J.-M. Beuken, F. Bottin, P. Boulanger, F. Bruneval, D. Caliste, R. Caracas, M. Ct, T. Deutsch, L. Genovese, P. Ghosez, M. Giantomassi, S. Goedecker, D. Hamann, P. Hermet, F. Jollet, G. Jomard, S. Leroux, M. Mancini, S. Mazevet, M. Oliveira, G. Onida, Y. Pouillon, T. Rangel, G.-M. Rignanese, D. Sangalli, R. Shaltaf, M. Torrent, M. Verstraete, G. Zerah, and J. Zwanziger, Comp. Phys. Commun. **180**, 2582 (2009), 40 YEARS OF CPC: A celebratory issue focused on quality software for high performance, grid and novel computing architectures.

42 N. Troullier and J. L. Martins, Phys. Rev. B 43, 1993 1444

(1991).
43 G. Kresse and J. Hafner, Phys. Rev. B **47**, 558 (1993).
44 G. Kresse and D. Joubert, Phys. Rev. B **59**, 1758 (1999).
45 P. E. Bl ochl, Phys. Rev. B **50**, 17953 (1994).
46 H. J. Monkhorst and J. D. Pack, Phys. Rev. B **13**, 5188 (1976).
47 M. Methfessel and A. T. Paxton, Phys. Rev. B **40**, 3616 (1989).
48 J. Neugebauer and M. Scheffler, Phys. Rev. B **46**, 16067 (1992).
49 L. Romaner, D. Nabok, P. Puschnig, E. Zojer and C. Ambrosch-Draxl, New J. Phys. **11** 053010 (2009).
50 P. Sony, P. Puschnig, D. Nabok, and C. Ambrosch-Draxl, Phys. Rev. Lett. **99**, 176401 (2007).
51 J. Klimes, D. R. Bowler, and A. Michaelides, J. Phys.: Condens. Matter **22**, 022201 (2010).
52 L. Kronik and A. Tkatchenko, Acc. Chem. Res. (2014), 10.1021/ar500144s.
53 S. Grimme, J. Comput. Chem. **27**, 1787 (2006).
54 G. Heimel, L. Romaner, J.-L. Bredas, and E. Zojer, Phys. Rev. Lett. **96**, 196806 (2006).
55 M. Rohlfing, R. Temirov, F. S. Tautz, Phys. Rev. B **76**, 115421 (2007).
56 F. S. Tautz, Progr. in Surf. Sci. **82**, 479 (2007).
57 G. Mercurio, O. Bauer, M. Willenbockel, N. Fairley, W. Reckien, C. H. Schmitz, B. Fiedler, S. Soubatch, T. Bredow, M. Sokolowski, F. S. Tautz, Phys. Rev. B **87**, 045421 (2013).
58 A. Hauschild, R. Temirov, S. Soubatch, O. Bauer, A. Schöll, B. C. C. Cowie, T.-L. Lee, F. S. Tautz, M. Sokolowski, Phys. Rev. B **81**, 125432 (2010).
59 Y. Zou, L. Kilian, A. Schöll, Th. Schmidt, R. Fink, and E. Umbach, Surf. Sci. **600**, 1240 (2006).
60 R. Schlaf, B. A. Parkinson, P. A. Lee, K. W. Nebesny, and N. R. Armstrong, J. Phys. Chem. B **103**, 2984 (1999).
61 S. Krause, M. B. Casu, A. Schöll, and E. Umbach, New J. Phys. **10**, 085001 (2008).
62 T. U. Kampen, Appl. Phys. A **82**, 457 (2006).
63 L. Kilian, A. Hauschild, R. Temirov, S. Soubatch, A. Schöll, A. Bendounan, F. Reinert, T.-L. Lee, F. S. Tautz, M. Sokolowski, and E. Umbach, Phys. Rev. Letters **100**, 136103 (2008).
64 At this point we have to add the following side note: For the HB/Ag(100) film no structural data about the vertical adsorption height is available, so we do not know how the HB/Ag(100) film fits into the picture. However, on the basis of the orbital binding energies and the above mentioned link to the adsorption heights (Fig. 4) we would expect that the adsorption distance of PTCDA in the HB structure on Ag(110) is in between that of BW/Ag(110) and T/Ag(100). Indeed, from general considerations regarding interface structure it is plausible that the adsorption height at the HB/Ag(110) is larger than at the BW/Ag(110) interface, because (1) increased intermolecular interactions between neighboring molecules (as are present in the HB phase) often lead to an increased molecule-substrate distance (this is known, e.g., from the comparison of high- and low-temperature phase of PTCDA on Ag(111); and (2), the loss of commensurability in going from the BW to the HB phase on Ag(110) also suggests a reduced molecule-substrate interaction and thus a larger adsorption height. Hence it appears as if the HB/Ag(110) film fits into the above mentioned tendency (i.e. orbital binding energy increases with adsorption height), if one remembers that here the effective reactivity of the surface is reduced by intermolecular interactions which enforce incommensurability.
65 A. Bondi, J. Phys. Chem. **68**, 441 (1964).
66 P. J. McGonigal , J. Phys. Chem. **66**, 1686 (1962).
67 I. Brown, J. Dimitz, Acta Cryst. **14**, 480 (1961).
68 G. V. Hansson and S. A. Flodström, Phys. Rev. B **18**, 1572 (1978).
69 H. C. Potter and J. M. Blakely, J. Vac. Sci. Technol. **12**, 635 (1975).
70 P. O. Gartland and B. J. Slagsvold, Phys. Rev. B **12**, 4047 (1975).
71 K. Giesen, F. Hage, F. J. Himpsel, H. J. Riess, and W. Steinmann, Phys. Rev. B **33**, 5241 (1986).
72 S. Duhm, A. Gerlach, I. Salzmann, B. Bröker, R. L. Johnson, F. Schreiber, and N. Koch, Organic Electronics **9**, 111 (2008).
73 A. W. Dweydari and C. H. B. Mee, phys. stat. sol. (a) **17**, 247 (1973).
74 M. Chelvayohan and C. H. B. Mee, J. Phys. C: Solid State Phys. **15**, 2305 (1982).
75 K. Giesen, F. Hage, F. J. Himpsel, H. J. Riess, W. Steinmann, and N. V. Smith, Phys. Rev. B **35**, 975 (1987).
76 W. Hansen, M. Bertolo, and K. Jacobi, Surf. Sci. **253**, 1 (1991).
77 A. W. Dweydari and C. H. B. Mee, phys. stat. sol. (a) **27**, 223 (1975).
78 B. Reihl and J. M. Nicholls, Z. Phys. B Condensed Matter **67**, 221 (1987).
79 M. Canepa, P. Cantini, L. Mattera, S. Terreni, and F. Valdenazzi, Physica Scripta **T41**, 226 (1992).
80 S. K. M. Henze, O. Bauer, T.-L. Lee, M. Sokolowski, F. S. Tautz, Surf. Sci. **601**, 1566 (2007).
81 A. Gerlach, S. Sellner, F. Schreiber, N. Koch, and J. Zegenhagen, Phys. Rev. B **75**, 045401 (2007).
82 A. Hauschild, K. Karki, B. C. C. Cowie, M. Rohlfing,

F. S. Tautz, M. Sokolowski, Phys. Rev. Lett. **94**, 036106 (2005).

83 I. G. Hill, A. Rajagopal, A. Kahn, and Y. Hu, Appl. Phys. Lett. **73**, 662 (1998).

84 I. G. Hill, A. Kahn, Z. G. Soos, R. A. Pascal, Jr., Chem. Phys. Lett. **327**, 181 (2000).

85 N. Dori, M. Menon, L. Kilian, M. Sokolowski, L. Kronik, and E. Umbach Phys. Rev. B **73**, 195208 (2006).

86 X. Blase, C. Attaccalite, and V. Olevano Phys. Rev. B **83**, 115103 (2011).

87 R. Hoffmann, Solids and Surfaces: A Chemists View of Bonding in Extended Structures (Wiley-VCH, New York, 1988).

88 D. M. Newns, Phys. Rev. **178**, 1123 (1969).

89 P. W. Anderson, Phys. Rev. **124**, 41 (1961).

90 J. K. Nørskov, Rep. Prog. Phys. **53**, 1253 (1990).

91 B. Hammer, Top. Catal. **37**, 3 (2006).

92 G. Mercurio, O. Bauer, M. Willenbockel, B. Fiedler, T. Sueyoshi, C. Weiss, R. Temirov, S. Soubatch, M. Sokolowski, F. S. Tautz, Phys. Rev. B **87**, 121409 (2013).

93 B. Stadtmüller, S. Schröder, F. C. Bocquet, C. Henneke, C. Kleimann, S. Soubatch, M. Willenbockel, B. Detlefs, J. Zegenhagen, T.-L. Lee, F. S. Tautz, and C. Kumpf, Phys. Rev. B **89**, 161407(R) (2014).

94 A. El-Sayed, P. Borghetti, E. Goiri, C. Rogero, L. Floreano, G. Lovat, D. J. Mowbray, J. L. Cabellos, Y. Wakayama, A. Rubio, J. E. Ortega, and D. G. de Oteyza, ACS Nano **7**, 6914 (2013).

95 E. Goiri, M. Matena, A. El-Sayed, J. Lobo-Checa, P. Borghetti, C. Rogero, B. Detlefs, J. Duvernay, J. E. Ortega, and D. G. de Oteyza, Phys. Rev. Lett. **112**, 117602 (2014).